

This work was written as part of one of the author's official duties as an Employee of the United States Government and is therefore a work of the United States Government. In accordance with 17 U.S.C. 105, no copyright protection is available for such works under U.S. Law.

Public Domain Mark 1.0

<https://creativecommons.org/publicdomain/mark/1.0/>

Access to this work was provided by the University of Maryland, Baltimore County (UMBC) ScholarWorks@UMBC digital repository on the Maryland Shared Open Access (MD-SOAR) platform.

Please provide feedback

Please support the ScholarWorks@UMBC repository by emailing scholarworks-group@umbc.edu and telling us what having access to this work means to you and why it's important to you. Thank you.

RESEARCH ARTICLE

10.1029/2018JD028313

Key Points:

- Major pollution events with high fine mode AOD in Eastern China and South Korea are often associated with significant cloud cover
- New AERONET Version 3 cloud screening allows more AOD observations in the near-cloud environment to be raised to Level 2
- MODIS satellite retrieval algorithms of AOD (collections 5 and 6.0) often screened out a significant number of high fine mode AOD days

Correspondence to:

 T. F. Eck,
 thomas.f.eck@nasa.gov

Citation:

Eck, T. F., Holben, B. N., Reid, J. S., Xian, P., Giles, D. M., Sinyuk, A., et al. (2018). Observations of the interaction and transport of fine mode aerosols with cloud and/or fog in Northeast Asia from Aerosol Robotic Network and satellite remote sensing. *Journal of Geophysical Research: Atmospheres*, 123, 5560–5587. <https://doi.org/10.1029/2018JD028313>

















Received 12 JAN 2018

Accepted 26 APR 2018

Accepted article online 4 MAY 2018

Published online 31 MAY 2018

Observations of the Interaction and Transport of Fine Mode Aerosols With Cloud and/or Fog in Northeast Asia From Aerosol Robotic Network and Satellite Remote Sensing

T. F. Eck^{1,2} , B. N. Holben¹, J. S. Reid³ , P. Xian³ , D. M. Giles^{1,4}, A. Sinyuk^{1,4} , J. S. Schafer^{1,4}, I. Slutsker^{1,4}, J. Kim⁵ , J.-H. Koo⁵, M. Choi⁵ , K. C. Kim⁶, I. Sano⁷, A. Arola⁸ , A. M. Sayer^{1,2} , R. C. Levy¹ , L. A. Munchak¹, N. T. O'Neill⁹, A. Lyapustin¹ , N. C. Hsu¹ , C. A. Randles^{1,10}, A. M. Da Silva¹, V. Buchard^{1,2} , R. C. Govindaraju^{1,4} , E. Hyer³ , J. H. Crawford¹¹ , P. Wang¹², and X. Xia¹² 

¹NASA Goddard Space Flight Center, Greenbelt, MD, USA, ²Universities Space Research Association, Columbia, MD, USA, ³Naval Research Laboratory, Monterey, CA, USA, ⁴Science Systems Applications, Inc., Lanham, MD, USA, ⁵Department of Atmospheric Sciences, Yonsei University, Seoul, South Korea, ⁶Gwangju Institute of Science and Technology, Gwangju, South Korea, ⁷Informatics Department, Kindai University, Osaka, Japan, ⁸Finnish Meteorological Institute, Kuopio, Finland, ⁹Centre d'Applications et de Recherches en Télédétection, Université de Sherbrooke, Sherbrooke, Quebec, Canada, ¹⁰Now at ExxonMobil Research and Engineering Company, Annandale, NJ, USA, ¹¹NASA Langley Research Center, Hampton, VA, USA, ¹²LAGEO, Institute of Atmospheric Physics, Chinese Academy of Sciences, Beijing, China

Abstract Analysis of Sun photometer measured and satellite retrieved aerosol optical depth (AOD) data has shown that major aerosol pollution events with very high fine mode AOD (>1.0 in midvisible) in the China/Korea/Japan region are often observed to be associated with significant cloud cover. This makes remote sensing of these events difficult even for high temporal resolution Sun photometer measurements. Possible physical mechanisms for these events that have high AOD include a combination of aerosol humidification, cloud processing, and meteorological covariation with atmospheric stability and convergence. The new development of Aerosol Robotic Network Version 3 Level 2 AOD with improved cloud screening algorithms now allow for unprecedented ability to monitor these extreme fine mode pollution events. Further, the spectral deconvolution algorithm (SDA) applied to Level 1 data (L1; no cloud screening) provides an even more comprehensive assessment of fine mode AOD than L2 in current and previous data versions. Studying the 2012 winter-summer period, comparisons of Aerosol Robotic Network L1 SDA daily average fine mode AOD data showed that Moderate Resolution Imaging Spectroradiometer satellite remote sensing of AOD often did not retrieve and/or identify some of the highest fine mode AOD events in this region. Also, compared to models that include data assimilation of satellite retrieved AOD, the L1 SDA fine mode AOD was significantly higher in magnitude, particularly for the highest AOD events that were often associated with significant cloudiness.

1. Introduction

The largest sources of uncertainty in the anthropogenic radiative forcing of climate are due to aerosol particles, both through direct forcing and also especially their indirect and/or semidirect effects on clouds (Intergovernmental Panel on Climate Change, 2013). At the same time, severe haze events have their own societal impacts with regard to human health, operations and transportation, and overall quality of life (e.g., Pope, 2000). Identifying and accurately quantifying the various climate and other societal effects of severe haze events has proved difficult both observationally and in atmospheric simulations. Observationally, there are some limitations to the separation of aerosol and cloud properties from passive satellite remote sensing retrievals of aerosol optical depth (AOD) due to cloud contamination of aerosol observations (Kaufman et al., 2005; Remer et al., 2013; Zhang et al., 2005) and due to reflected radiation from the sides of clouds into the aerosol field, thereby enhancing the apparent aerosol signal (e.g., the 3-D radiative cloud adjacency effect; Marshak et al., 2008; Várnai & Marshak, 2009). Passive satellite algorithms often identify high concentration aerosol events as clouds and therefore fail to perform AOD retrievals (Shi, 2015). Severe haze events frequently also have stratocumulus cloud elements. Finally, haze events have a high degree of spatial and temporal variability. Ultimately, severe haze events represent the physical continuity between “aerosol particle” and “cloud droplet” including all of the strong nonlinearities associated with aerosol

and cloud microphysics, secondary aerosol production, and the overall meteorological environment. Compounding the complexity of the physics is the nature of satellite observing systems themselves and each sensor's strengths and challenges. As shown in studies in Southeast Asia, wide divergences exist in cloud and aerosol products (e.g., Reid et al., 2013) with each observing one limited aspect of the environment. The above issues often make it difficult to accurately observe the near-cloud aerosol environment. Vertical profiling observations from lidars may overcome and/or minimize some of these issues but residual cloud contamination may remain, and lidar beams can be completely attenuated in high AOD. Nevertheless, several studies utilized spaceborne Cloud-Aerosol Lidar and Infrared Pathfinder Satellite Observation lidar data (Tackett & Di Girolamo, 2009; Várnai & Marshak, 2011; Yang et al., 2012) and aircraft based high spectral resolution lidar data (Su et al., 2008) to investigate aerosol near-clouds finding significant enhancements in the vicinity of low-altitude clouds.

Models have even more difficulty in coping with severe haze events. Indeed, severe haze in the Indo-Gangetic Plain and in the North China Plain (NCP) pose the most significant challenging air mass regimes for global aerosol models (Sessions et al., 2015). The models' requirement to resolve shallow moist boundary layer, strong subsidence, and stratocumulus clouds coupled with strong nonlinearity in particle hygroscopicity with high relative humidity (RH) is daunting. AOD data assimilation (DA) only marginally improve the situation, as the input observations and the modeling alike suffer from the same shortcomings as noted above. Dynamic uncertainties in the model subsequently lessen the impact of DA in forecast time.

For both observations and modeling simulations meteorological covariation with severe haze can be a particularly difficult issue to accurately quantify due to the possibility of several simultaneous effects such as aerosol humidification in the high RH environment in the vicinity of clouds, cloud processing of existing aerosols (Dall'Osto et al., 2009; Hoppel et al., 1994; Munger et al., 1986; Noone et al., 1992), and secondary particle production to sulfate, nitrate, and organic aerosol (Ervens et al., 2011; Hansen et al., 1991; Hayden et al., 2008). Simulation studies by Quaas et al. (2010) and Grandey et al. (2013) utilized general circulation models to conclude that aerosol humidification or swelling in high RH regions in the vicinity of clouds was the dominant factor in the model's relationship between AOD and total fractional cloud cover. More recently, Gryspeerd et al. (2016) analyzed satellite data, taking into account cloud droplet number concentration and concluded that the global mean AOD and cloud fraction relationship is reduced by 80% when meteorological covariation is taken into account. Additionally, increases in aerosols may increase cloud fraction by extending cloud lifetimes as a result of decreasing cloud droplet size, thereby delaying precipitation (Albrecht, 1989).

An early step in assessing the nature of haze events is to determine their probability of formation and then uniformly evaluating the satellite aerosol products and models. From a direct radiative forcing assessment point of view, monitoring the regional ambient aerosol optical state with Sun photometers is one way to unambiguously characterize the total integrated atmospheric aerosol column. Due to their small fields of view, there is no significant 3-D radiative adjacency effect in Sun photometer data when measurements of AOD are made in close proximity to clouds, and the much higher effective temporal resolution, such as from instruments in the Aerosol Robotic Network (AERONET), allows for monitoring of haze evolution throughout the day with much less potential cloud contamination. In Sun photometer measurements the small field of view (FOV) insures that the signal is dominated by the direct Sun signal with minimal contribution of diffuse radiation (which could originate from cloud multiple scattering) within the FOV. Sinyuk et al. (2012) analyze the effect of diffuse in the FOV for the AERONET Sun-sky radiometers utilized in this study. The spectral deconvolution algorithm (SDA; O'Neill et al., 2003; Kaku et al., 2014), which separates fine and coarse mode AOD, further isolates potential cloud droplets from fine mode particles, including larger haze (cloud processed) particles (Eck et al., 2012). This allows for improvement in the overall observability of the fine mode aerosol system (e.g., Arola et al., 2017).

Aerosol-cloud covariance can come through transport covariance and more "local" cloud effects. For example, transport covariance between significant aerosol outbreaks and synoptic-scale frontal cloud features in Asia has been reported (Zhang & Reid, 2009). More interest in the scientific community, however, has been toward local aerosol-cloud relationships. For example, Zhang et al. (2005) and Jeong and Li (2010) examined satellite and Sun photometer-derived AODs for marine and continental clouds, respectively. These studies used different algorithms and measurement types (satellite and Sun-sky radiometers) to determine what a cloud is, typically by spatial and/or temporal variance (assuming clouds cause larger variance than

aerosols) and not by particle size or chemical composition. The findings of Zhang et al. (2005) suggest that 70% of the increased satellite signal in AOD in the vicinity of marine clouds is due to cloud contamination, with the remaining 30% due to hygroscopicity or secondary production. For clouds in Oklahoma, Jeong and Li (2010) found, from both AERONET Sun photometer and aircraft in situ data, enhanced AOD near clouds and that only ~25% of the enhancement was due to humidification, while most was due to the combined effects of new particle formation, cloud processing of particles, and convergence of air in clouds. Eck et al. (2012) presented evidence of aerosol growth through cloud processing after the evaporation of extensive fog or low-altitude stratus (layer) clouds, with retrieved size distributions from AERONET showing submicron mode bimodality similar to that measured by various in situ field measurements. Furthermore, Eck et al. (2014) found rapid and sometimes large (doubling at times) increases in fine mode AOD in the immediate vicinity of nonprecipitating polluted cumulus clouds from AERONET measurements in the mid-Atlantic U.S. region. Since there often was no significant change in retrieved particle size or Ångström exponent associated with these increases in AOD, this suggests possible secondary particle production in cloud droplets and/or hygroscopic growth of exiting subvisible Aitken size particles into the optically effective accumulation mode in addition to hygroscopic growth and cloud processing of existing accumulation mode size particles. Both aircraft in situ and high spectral resolution lidar measurements were consistent with the AERONET measured increases in AOD near these cumulus clouds and additionally consistent in the overall lack of change in fine mode particle size parameters.

Recent research focused on East Asian haze events provides an opportunity for understanding not only their nature but their observability and predictability as well. During March–June 2012 a regional AERONET field experiment in South Korea and Japan provided an opportunity to investigate remote sensing signals of aerosol optical properties. In the current paper we analyze the AERONET measurements of AOD during this field campaign in addition to an upwind site in the Northern China Plain (east of Beijing), focusing in particular on the fine mode AOD retrieved by SDA and especially focusing on measurements in the nearby vicinity of clouds or data that were eliminated by cloud screening algorithms. Additionally, we examine the retrievals of AOD from satellite by Moderate Resolution Imaging Spectroradiometer (MODIS) sensors from three different retrieval algorithms and compare these to the AERONET retrieved fine mode AOD. Fine mode AOD estimated by aerosol reanalyses (Buchard et al., 2015; Lynch et al., 2016) are also compared to the fine mode AOD from AERONET for selected sites. Finally, we investigate the monthly mean AOD climatology from AERONET at sites in both China and South Korea, specifically analyzing the differences in fine mode AOD from cloud-screened versus non-cloud-screened data.

This paper primarily analyzes the Version 2 AERONET data that have been utilized in all AERONET data analyses from 2006 to 2016, since the vast majority of the published literature to date have utilized AERONET Version 2 data. The recently developed Version 3 is also examined in the context of relative differences between Version 2 and Version 3 AOD for selected sites and time intervals since the new cloud-screening algorithm is significantly different in Version 3 as compared to Version 2. However, more extensive comparisons of Versions 2 and 3 AOD data sets will be the topic of future investigations.

2. Instrumentation, Data, and Methodology

For the Distributed Regional Aerosol Gridded Observation Network (DRAGON)-Korea and DRAGON-Japan 2012 networks, there were 22 AERONET Cimel Sun-sky radiometer sites in a mesoscale DRAGON in South Korea (11 of these in the greater Seoul metropolitan area) and 14 Cimels in Japan in the spring and summer of 2012 (Holben et al., 2018; Lee & Son, 2016; Sano et al., 2016). These site deployments included existing AERONET long-term monitoring sites in both South Korea and Japan. However, only a subset of these sites were analyzed in detail since many sites were clustered in urban centers (Greater Seoul in South Korea and Osaka in Japan) and therefore showed very similar time series of AOD to each other. Additionally, the occurrence of the field campaign insured that the long-term monitoring stations would be operating well during this time interval.

2.1.1. AERONET Instrumentation

The CIMEL Electronique CE-318 Sun-sky radiometer measurements were made with instruments that are a part of the AERONET global network. These instruments are described in detail by Holben et al. (1998); however, a brief description is given here. The automatic tracking Sun and sky scanning radiometers made direct Sun measurements with a 1.2° full FOV every 15 min at 340, 380, 440, 500, 675, 870, 940, and 1,020 nm (nominal wavelengths; includes the 1,640-nm channel in extended wavelength Cimel versions). It is noted that for this campaign several Cimels were operated with a 3-min sampling interval to obtain higher temporal

resolution data, much more frequent than the standard 15-min interval of AERONET. The direct Sun measurements take ~ 8 s to scan all wavelengths (repeated three times within a minute), with a motor driven filter wheel positioning each filter in front of the detector. These solar extinction measurements are used to compute AOD at each wavelength except for the 940-nm channel, which is used to retrieve total column water vapor (or precipitable water) in centimeters. The filters utilized in these instruments were ion assisted deposition interference filters with band pass (full width at half maximum) of 10 nm, except for the 340- and 380-nm channels at 2 nm. The estimated uncertainty in computed AOD, due primarily to calibration uncertainty, is ~ 0.010 – 0.021 for field instruments (which is spectrally dependent with the higher errors in the ultraviolet; Eck et al., 1999). Schmid et al. (1999) compared AOD derived from four different solar radiometers (including an AERONET Sun-sky radiometer) operating simultaneously together in a field experiment and found that the AOD from 380 to 1,020 nm agreed to within a root-mean-square (RMS) difference of 0.015, which is similar to our estimated level of uncertainty in AOD measurements for field instruments.

For some of the analyses presented, the Version 2 spectral AOD data have been screened for clouds following the methodology of Smirnov et al. (2000), which relies on the higher temporal frequencies of cloud optical depth (COD) as compared to AOD, especially optical depth triplet variability within 1 min. Triplet variability is defined as the maximum minus minimum AOD of the three values taken in a 1-min time interval for each wavelength, with all spectral channels being checked for triplet range. AOD measurements pass the Version 2 cloud screening when triplet variability is less than either 0.02 or $0.03 \times \text{AOD}$ (whichever value is higher), and the measurement is screened if any wavelength triplet variability exceeds the threshold. In the newer Version 3 cloud screening, only three channels (675 nm, 870, and 1,020 nm) are checked for triplet variance, and the measurement is screened when the triplet range for all three wavelengths exceeds 0.01 or $0.015 \times \text{AOD}$ (whatever is greater). The complete set of Version 3 cloud screening and quality assurance (QA) algorithms are provided in another AERONET publication in preparation (D. Giles, personal communication, May 4, 2018). The sky radiances measured by the Sun/sky radiometers are calibrated versus frequently characterized integrating spheres at the National Aeronautics and Space Administration (NASA) Goddard Space Flight Center, to an absolute accuracy of $\sim 5\%$ or better (Holben et al., 1998).

2.1.2. Spectral Deconvolution Algorithm

Based on the assumption that aerosol size distributions are bimodal, O'Neill et al. (2001, 2003) developed the SDA that utilizes spectral total AOD data to infer the component fine and coarse mode optical depths. An additional fundamental assumption of the algorithm is that the coarse mode Ångström exponent and its derivative are both close to 0, which is based on Mie calculations for coarse mode particles that are assumed to have supermicron radii. The Ångström exponent α and the spectral variation of α (as parameterized by $\alpha' = d\alpha/d\ln\lambda$) are the measurement inputs to the SDA. These continuous-function derivatives (computed here at a reference wavelength of 500 nm) are derived from a second order fit of \ln AOD versus $\ln \lambda$ (Eck et al., 1999). For purposes of consistency with prior literature, in this study we report the classical AERONET 440- to 870-nm Ångström exponent rather than the spectral derivative at 500 nm. The measured spectral AODs employed as input to the SDA were limited to the five CIMEL wavelengths ranging from 380 to 870 nm, and in this study all channels must have been available for the retrievals even though this is not a requirement for Level 2 data. An additional quality control check was utilized in this study to ensure high-quality Level 1 data: we only analyzed Level 1 data when Level 2 data were available in the same week. The AERONET data in Level 1 were not screened for clouds, since O'Neill et al. (2003) have shown that SDA incorporates COD into the coarse mode AOD component. Due to far forward scattering by ice, the perceived COD from Sun photometry is less than the actual. Nevertheless, the analysis by Chew et al. (2011) of AERONET measured spectral AOD in conjunction with lidar data in Singapore has shown that the SDA technique effectively separated the fine mode AOD component from the total optical depth with a cirrus cloud contamination coarse mode. Additionally, Kaku et al. (2014) have verified that the SDA technique is also effective in separating the fine and coarse modes from in situ spectral optical measurements. However, although the Level 1.0 AOD data do not have the AERONET cloud-screening algorithm of Smirnov et al. (2000) applied, there is still a basic filter of large temporal variance of the signal applied to all Level 1.0 data. The direct Sun measurement data are not included in the AERONET Level 1.0 data set if the variance of the raw signal is very high within the triplet sequence. The variance threshold applied is based on the RMS differences of

the three direct Sun triplet measurements relative to the mean of these three values. If the (RMS/mean)-100% of the triplet values is greater than 16%, then the data are not used for computation of AOD and do not appear in the Level 1.0 data set. This temporal variance threshold primarily removes data that are affected by clouds with large spatial-temporal variance in COD. This effectively removes much of the cumulus cloud contaminated data, although some of the thinner edges with lower COD do remain in the data (see in Eck et al., 2014, the decreases in Ångström exponent in Figure 6b and the increases in coarse mode AOD in Figure 8b, for example).

The AERONET Level 1 total optical depth uncertainty in the visible and near infrared is ~ 0.01 after final calibrations are applied and if Level 2 exists for the same time interval. This is the same uncertainty as Level 2 AOD since it is determined primarily by radiometer calibration. The uncertainty in fine AOD in Level 1 data mainly arises from the separation of fine versus coarse mode in the total optical depth (when thin cloud contaminates the data) or in total AOD when there is no cloud contamination. The definition of the aerosol fine and coarse modes varies between different approaches. For example, the Dubovik and King (2000) almucantar retrieval approach defines the two modes as the local minima in size distribution between the two modes (for volume radius ranging from 0.44 to 0.99 μm), while in the O'Neill et al. (2003) SDA algorithm the two modes include the tails of the size distributions with no radius cutoff to define the modes. The fine mode fraction (FMF) from the SDA is lower than that from the Dubovik retrieval by ~ 0.05 (Eck et al., 2010) likely due in large part from this difference in definition between modes. Therefore, in this paper the high fine mode AOD cases identified by SDA that are screened as clouds by the AERONET algorithms may actually have somewhat higher fine mode AOD as determined by different fine versus coarse mode definitions.

2.1.3. AERONET Inversion Methodology

In addition to AOD from direct Sun measurements, the CIMEL collects sky radiance measurements in the almucantar geometry (fixed elevation angle equal to solar elevation, and $\pm 180^\circ$ azimuthal sweeps) at 440, 675, 870, and 1,020 nm (nominal wavelengths). Both types of measurement are used together to retrieve optical equivalent, column integrated aerosol size distributions, and refractive indices. Using this microphysical information, the spectral dependence of single scattering albedo (SSA) is calculated. The algorithm of Dubovik and King (2000) with enhancements detailed in Dubovik et al. (2006) was utilized in these retrievals, known as Version 2 AERONET almucantar retrievals. Only Version 2 Level 2 quality assured almucantar retrievals (Holben et al., 2006) are presented in this paper, unless otherwise noted. The Version 2 AERONET algorithm determines the percentage of spherical and spheroidal particles required to give the best fit to the measured spectral sky radiance angular distribution. Further details on the Version 2 algorithm and the improved specification of surface bidirectional reflectance can be found in Dubovik et al. (2006) and Eck et al. (2008).

Almucantar sky radiance measurements were made at optical air masses of 4, 3, 2, and 1.7 (75° , 70° , 60° , and 54° solar zenith angle [SZA], respectively) in the morning and afternoon and once per hour in between. In order to ensure sky radiance data over a wide range of scattering angles, only almucantar scans at SZAs greater than $\sim 50^\circ$ are analyzed and presented here. In order to eliminate cloud contamination from the almucantar directional sky radiance data, AERONET requires the radiances to be symmetrical on both sides of the Sun at equal scattering angles, and symmetric radiances from both sides are subsequently averaged. Directional sky radiance measurements that are not symmetrical (due to cloud on one side or inhomogeneous aerosol distribution) are eliminated, and the minimum number of measurements required in given scattering angle ranges for a Level 2 retrieval are shown in Holben et al. (2006).

The stable performance of the inversion algorithm was illustrated in sensitivity studies performed by Dubovik et al. (2000) where the perturbations of the inversion resulting from random errors, possible instrument offsets and known uncertainties in the atmospheric radiation model were analyzed. Their work employed retrieval tests using known size distributions to demonstrate successful retrievals of mode radii and the relative magnitude of modes for various types of bimodal size distributions such as those dominated by a submicron accumulation mode or distributions dominated by supermicron coarse mode aerosols. Although very few direct comparisons of size distribution between in situ and AERONET retrievals have yet been published, there are several aerosol types in specific regions that have been or can be compared. For example, Reid et al. (2005) present a table where the volume median radius of smoke from various major biomass

burning regions (South America, southern Africa, and North America [boreal and temperate]) is compared. For all three of these regions, the volume median diameters of the in situ versus the AERONET retrievals are often within $\sim 0.01 \mu\text{m}$ of each other. Similarly, for fine mode pollution in the Arabian Sea during the Indian Ocean Experiment, Clarke et al. (2002) presented lognormal fits of volume size distributions from aircraft and ship in situ instrument measurements that showed average accumulation mode volume peak radius values of $0.17\text{--}0.18 \mu\text{m}$ with geometric standard deviations of 1.43 (aircraft) and 1.51 (ship) for observations made under high aerosol scattering conditions. This compares well with retrievals made at Kaashidhoo Island, Maldives (in the same region), when $\text{AOD}(440 \text{ nm}) > 0.4$, of $0.18\text{-}\mu\text{m}$ median radius and width of 1.49 (AERONET Version 2 averages from 1998 to 2000). For larger submicron-sized aerosols, Eck et al. (2010) discussed the relatively close agreement for Pinatubo stratospheric aerosol observations of $\sim 0.56\text{-}\mu\text{m}$ peak volume radius from AERONET retrievals to $0.53\text{-}\mu\text{m}$ effective radius from in situ stratospheric aircraft measurements, as reported by Pueschel et al. (1994). In the coarse mode (supermicron radius), Reid et al. (2006) and Reid et al. (2008) showed excellent agreement between in situ measured size and AERONET retrievals for sea salt and desert dust, respectively. Smirnov et al. (2003) showed reasonable agreement between AERONET retrievals of size distributions and in situ measurements for aerosols of marine origin. Similarly, Johnson and Osborne (2011) have shown good agreement between aircraft in situ measured size distributions and AERONET retrievals for coarse mode dust in the Sahel region of West Africa.

2.1.4. MODIS Satellite Retrievals of AOD

MODIS is a spaceborne passive imaging radiometer that flies on two satellite platforms: Terra with data from mid-2000 to present and a daytime node equatorial solar crossing time around 10:30 a.m. and Aqua with data from late 2002 to present and a daytime node equatorial solar crossing time around 1:30 p.m. as part of the A-Train constellation. The instruments have the same basic characteristics but have aged differently in flight (e.g., Lyapustin et al., 2014; Toller et al., 2013). They measure reflected solar and emitted thermal radiation in 36 bands in the spectral range 412 nm to $14.3 \mu\text{m}$, with nominal horizontal pixel sizes at the center of swath from 250 m to 1 km (dependent on band). Due to MODIS's scan geometry and the shape of the Earth pixel sizes become increasingly larger, and shapes distorted, for off-nadir view angles (see Sayer, Hsu, & Bettenhausen, 2015, for the impacts of this so-called "bow tie effect" on the aerosol products). Several algorithms have been developed and applied by NASA to provide AOD at 550 nm as part of MODIS routine data processing. A summary of the key features of those used herein is provided below. MODIS data versions are known as "Collections," each being a full-mission reprocessing for a particular science discipline with consistent algorithms and calibration applied to the whole records to avoid discontinuities. The most recent full Atmospheres discipline reprocessing is Collection 6 (C6); an updated Collection 6.1 (C6.1) reprocessing is ongoing at present, although the cores of the algorithms are similar to those of C6.

2.1.4.1. Dark Target Algorithm

MODIS Dark Target (DT) consists of two distinct algorithms: one applied over-land and the other over-water pixels. The C6 products are described by Levy et al. (2013). In brief, the main data product from both is the AOD at 550 nm ; particle size-related information is also provided over water but not over land, as that aspect of the retrieval was found to have little skill in the latter case. Both land and ocean products are generated with a Level 2 pixel size of nominally $10 \times 10 \text{ km}^2$ at the center of the swath. Cloud screening is applied at sensor pixel resolution; after cloud masking, a proportion of additional pixels are discarded, and then the remaining top of atmosphere (TOA) reflectances averaged, with this average spectral TOA reflectance used in the retrieval. QA tests use (among other things) the number of such available pixels to assign each retrieval a QA value from 0 (*poorest*) to 3 (*best*). Over land it is recommended that only QA = 3 retrievals are used, and over water only QA > 0 retrievals are used. This QA filtering is applied to create the data set Optical_Depth_Land_And_Ocean that is provided in the aerosol data products, which are denoted MOD04 for data from MODIS Terra and MYD04 for data from MODIS Aqua. The non-QA-filtered equivalent data set is Image_Optical_Depth_Land_And_Ocean. Versions of the DT algorithms have also been applied to Visible Infrared Imaging Radiometer Suite measurements (Levy et al., 2015).

The over-land DT algorithm is based on the principle that by using shortwave infrared (swIR) bands, where the atmospheric contribution to the TOA signal is dark the surface reflectance in certain visible bands (centered near 470 and 650 nm) can be estimated. This is done using an empirical relationship based on a swIR vegetation index together with Sun/view geometry information (Levy et al., 2007), although the

relationship only holds for vegetated surfaces (i.e., dark surface targets) and so the retrieval is not performed over bright surfaces such as deserts, bare soil, or snow/ice. The AOD at 550 nm is then retrieved by using these surface reflectances and varying the abundances of two aerosol models (both bimodal; one dominated by fine mode aerosols, with properties dependent on region and season, and the other coarse mode dominated, to represent mineral dust) in order to match the observed TOA reflectance.

The over-water DT algorithm models surface reflectance as a function of near-surface wind speed. Aerosols are modeled by considering combinations between one of four fine mode components and one of five coarse mode components. For each of the resulting 20 fine/coarse mode pairs, the algorithm determines the AOD at 550 nm and a fine/coarse mode aerosol weighting by varying the abundances of these aerosol components to match the observed TOA reflectance. Both best fit solutions, and the average of all solutions matching the TOA reflectance to within a certain threshold, are provided in the retrieval products; the latter (average solution) is that which is used in most cases (including here).

The uncertainty of the over-land DT retrievals is expressed as an expected error (EE) envelope in which one standard deviation (around 68%) of retrieved AODs lie relative to the truth. These limits have been established based on validation against AERONET direct-Sun observations (Levy et al., 2013; Sayer et al., 2014, for C6), and are diagnostic (i.e., defined relative to AERONET). Over land, the EE is of order $0.05 + 15\%$, while over water, the envelope is asymmetric and between $(-0.02-10\%)$ and $(0.04 + 10\%)$.

2.1.4.2. Deep Blue Algorithm

A motivation for the original development of Deep Blue (DB) was to fill in gaps in the MODIS DT over-land data products from bright desert/soil surfaces, since these are important source regions for large parts of the global aerosol system, particularly mineral dust (Hsu et al., 2004, 2006). In C6 (Hsu et al., 2013), DB was extended to cover all cloud-free land surfaces (except for snow/ice). Versions of DB have also been applied to Advanced Very High Resolution Radiometer, Sea-viewing Wide Field-of-view Sensor, and Visible Infrared Imaging Radiometer Suite measurements. The DB retrievals are provided alongside DT in the MOD04/MYD04 aerosol products. A merged DB/DT data set is also provided (Sayer et al., 2014), although this is not discussed here since the aim is to examine the individual algorithms.

The DB algorithm uses different techniques to estimate surface reflectance based on the underlying surface type. For bright surfaces such as deserts, surface reflectance changes comparatively slowly in time and so a surface database is used. This database is constructed using a modified version of the minimum reflectance technique, performing a correction for Rayleigh scattering and an assumed background aerosol level, and aggregates observations from over both MODIS records. The data are then binned by season, scattering angle, and normalized difference vegetation index to create databases at 0.1° horizontal resolution for the MODIS bands centered near 412, 470, and 650 nm (Hsu et al., 2013). The physical principle behind the retrieval is that some "bright" surfaces such as deserts are, in fact, comparatively dark in the blue spectral region. Thus, the "deep blue" band (412 nm), which gives the algorithm its name, is used to retrieve the AOD at that wavelength. The 470-nm band is used to provide additional retrieval of AOD at 470 nm. These are used together to provide AOD at 550 nm and Ångström exponent, although if the 470-nm AOD is below 0.2, then the Ångström exponent is set to a fixed value and only AOD is retrieved. If internal tests indicate the presence of heavy mineral dust in a pixel, then the 650-nm band is also used and aerosol SSA is retrieved using a maximum likelihood method to pick between one of a candidate set of SSA spectral shapes (Hsu et al., 2013). Over vegetated surfaces, the assumption that surface reflectance varies slowly in time is not valid. In these cases the algorithm uses empirical spectral/directional relationships between the swIR and visible bands (using the same physical principles as the DT approach) and instead uses the 470- and 650-nm bands to retrieve AOD at 550 nm and Ångström exponent.

Aerosol optical properties are set based on region and season and are the same for both the bright and dark surface algorithm paths. A key difference between DT and DB is that DT averages cloud-free reflectances within the 10-km retrieval pixel and then does a retrieval, while DB retrieves on each suitable cloud-free 1-km pixel and then averages the retrieved AOD and Ångström exponent to the 10-km grid. Thus, it is possible for a 10-km retrieval pixel to contain inputs from both the bright and dark surface methods. DB also has QA tests (based on pixel availability within the 10-km pixel and its neighbors and the variability of the retrieved AOD field within the pixel). All retrievals are provided within the data set `Deep_Blue_Aerosol_Optical_Depth_550_Land`, but in most cases it is recommended only to use QA = 2 or

QA = 3 retrievals, which are used to populate Deep_Blue_Aerosol_Optical_Depth_550_Land_Best_Estimate; both are used in this analysis. It is important to note that QA tests and definitions are not the same between DB and DT land or ocean algorithms, despite the common nomenclature.

The C6 DB retrievals have also been validated (Sayer et al., 2013, 2014, for Aqua; Sayer, Hsu, Bettenhausen, et al., 2015, for Terra). The usual quoted global average EE is $0.03 + 20\%$, although prognostic uncertainty estimates have been developed and are included on a pixel level in the MODIS aerosol data products. Generally, errors are smaller over vegetated surfaces than arid ones and (slightly) smaller for MODIS Aqua retrievals than MODIS Terra (Sayer et al., 2013; Sayer, Hsu, Bettenhausen, et al., 2015). There is at present no DB over-water data set provided within the MODIS aerosol product distribution.

2.1.4.3. MAIAC Algorithm

The Multi-Angle Implementation of Atmospheric Correction (MAIAC) algorithm uses a physical atmosphere-surface model where the model parameters are defined from measurements (Lyapustin, Martonchik, et al., 2011; Lyapustin, Wang, et al., 2011, 2012; Lyapustin, Korkin, et al., 2012). Instead of swath-based processing, MAIAC starts by gridding MODIS L1B measurements to a fixed 1-km grid and by accumulating a time series of data for up to 16 days using a sliding window technique. This allows MAIAC to observe the same grid cell over time, helping separate atmospheric and surface contributions with the time series analysis and characterize surface bidirectional reflectance distribution function using multiangle observations from different orbits. Besides bidirectional reflectance distribution function retrieval, the fixed (gridded) surface representation allows characterization of unique surface spectral, spatial, thermal, etc. signatures for each 1-km grid cell, helping to improve cloud and snow detection, aerosol retrievals, and atmospheric correction.

Similarly to the DT method, MAIAC uses MODIS swIR (2.1 μm) measurement to predict surface reflectance at 470 nm, with AOD retrieval based on matching the measured TOA reflectance. However, the spectral ratio of surface reflectance between these two bands is defined from measurements using a modified minimum reflectance method, rather than using a statistically averaged empirical spectral/directional relationship as DT does. Over bright surfaces, aerosol retrieval additionally uses a green band (550 nm).

Currently, MAIAC uses eight different regional aerosol optical models over land globally. Smoke/dust detection is synergistic with MAIAC's cloud mask, helping to retain high-contrast fire smoke plumes at 1-km resolution in the AOD product with minimal cloud leakage and also helping to select the proper optical model for the AOD retrieval.

MAIAC reports AOD at gridded 1-km resolution at two wavelengths, 470 nm where the original retrieval is made, and interpolated at 550 nm based on the selected aerosol model. The 550-nm value was added for compatibility with the standard AOD products, as well as to support modeling and application analysis commonly using this wavelength. The AOD accuracy is generally similar at the two wavelengths, though it is slightly higher at 470 nm. Along with AOD, MAIAC provides prognostic uncertainty as a function of surface brightness, which is modulated by the view geometry, and the QA flag mostly indicating proximity to detected clouds or snow. The recommended QA values are 0 and 1 to obtain the best quality AOD.

The MAIAC MODIS Collection 6 (with enhanced calibration (C6+), which added polarization correction of MODIS Terra, removed residual trends of both Terra and Aqua and cross-calibrated Terra to Aqua; (Lyapustin et al., 2014) reprocessing started in September 2017 using the MODIS Adaptive Processing System. It is expected to be completed in 4–6 months creating a new MODIS product MCD19 accessible via Land Product Distributed Active Archive Center. Several studies are currently conducting global evaluation of MAIAC AOD. Regional AERONET-based validation over North and South America is available from Superczynski et al. (2017) and Martins et al. (2017), respectively.

2.1.5. Data Assimilation Models

2.1.5.1. NAAPS Model

In this analysis we make use of the Navy Aerosol Analysis and Prediction System-Reanalysis (NAAPS, Lynch et al., 2016). This reanalysis is based on the operational version of NAAPS (<http://www.nrlmry.navy.mil/aerosol/>), run at the U.S. Navy's Fleet Numerical Meteorological and Oceanographic Center, but with more consistent meteorology, source/sink, and DA procedures throughout the reanalysis time. Four mass-based aerosol source species and one gas species are included in the model, including sea salt, dust, and biomass burning.

A combined anthropogenic and biogenic fine species is run with SO₂ to account for the complex and often collinear behavior of sulfate, organic species, and black carbon species. Smoke from biomass burning is derived from near-real-time satellite-based thermal anomaly data used to construct smoke source functions (Reid et al., 2009), with additional orbital corrections on MODIS based emissions. Dust is emitted dynamically (Westphal et al., 1987) and is a function of modeled friction velocity to the fourth power, surface wetness, and surface erodability, which is adopted from Ginoux et al. (2001) with regional tuning. Sea-salt modeling is the same as Witek et al. (2007), and sea-salt emission is driven dynamically by sea surface wind. The reanalysis is run off-line from a 1° × 1° latitude-longitude resolution at 30 levels truncation of the Navy Global Environmental Model (Hogan et al., 2014). The satellite-derived National Oceanic and Atmospheric Administration Climate Prediction Center MORPHing (Joyce et al., 2004) precipitation is used to constrain aerosol wet removal within the tropics (Xian et al., 2009). A fused AOD product of specially derived and corrected quality controlled MODIS Level 3 C5 data (Hyer et al., 2011; Zhang & Reid, 2006) and likewise Multiangle Imaging Spectroradiometer AOD data (Shi et al., 2014) are assimilated via the Navy Atmospheric Variational Data Assimilation System for AOD (Zhang et al., 2008). The overall correlation between NAAPS reanalysis and AERONET observations is comparable to that of the satellite aerosol products themselves (Lynch et al., 2016; Zhang et al., 2008). The reanalysis also reproduces the decadal AOD trends found using standalone satellite products in other studies (Lynch et al., 2016).

2.1.5.2. MERRAero

The MERRA Aerosol Reanalysis (MERRAero; Buchard et al., 2015, 2016) is an off-line aerosol reanalysis in which bias-corrected MODIS AOD is assimilated into a version of the NASA Global Earth Observing System, Version 5 model (GEOS-5). As described in Buchard et al. (2015), for MERRAero, GEOS-5 is run in “replay” mode, in which a previous meteorological analysis is used to adjust the model’s state (winds, temperature, and specific humidity), much like in a chemical transport model, but with aerosol transport dynamics that are consistent with the model’s thermodynamic state. In MERRAero, GEOS-5 is replayed from meteorology from the Modern-Era Retrospective Analysis for Research and Applications, Version 1 (MERRA-1; Rienecker et al., 2011). The Goddard Chemistry, Aerosol, Radiation and Transport Model (Chin et al., 2002; Colarco et al., 2010) is coupled to GEOS-5 to simulate the sources, sinks, and chemistry of 15 externally mixed aerosol mass mixing ratio tracers (five dust bins, five sea-salt bins, hydrophobic and hydrophilic black and organic carbon, and sulfate). Then, by means of AOD analysis splitting (see Randles et al., 2017, for technical details), MERRAero assimilates bias-corrected AOD observations from MODIS (both Terra and Aqua, C5 version). The bias-correction algorithm uses a neural network to cloud screen, homogenize, and translate MODIS reflectances into AERONET-calibrated AOD. This postprocessing of the MODIS observations helps to reduce biases in the AOD assimilation relative to independent AOD observations, as shown by Saide et al. (2013). MERRAero Aerosol Absorption Optical Depth and aerosol index were validated with independent observations from the Ozone Monitoring Instrument (Buchard et al., 2015), and PM_{2.5} were validated with ground observations from the Environmental Protection Agency (Buchard et al., 2016).

3. Results

3.1. Cloud Screening of Fine Mode Aerosol Events—Daily Averages

In this section we examine large-magnitude fine mode AOD events and the cloud screening of some of these events that are associated with extensive cloud cover environments. We will first examine the impacts of Version 2 cloud screening and then compare with the new Version 3. The AERONET Version 2 database SDA fine mode AOD Level 1 (no cloud screening) versus Level 2 (cloud screened) daily average AOD comparisons for four sites for winter-summer 2012 are presented in Figure 1. Version 2 cloud screening of AOD data (L2) eliminates many major fine mode AOD events (primarily pollution events) with high AOD (500 nm) > 1.0 at several sites in this East Asian region, including Yonsei University, South Korea, Baengnyeong, South Korea, XiangHe, China, and Fukuoka, Japan (red diamonds without a corresponding black bar, shown in Figure 1). Many of these high fine mode AOD days that were cloud screened have very few observations of AOD per day (typically due to high cloud fraction seen at MODIS overpasses). Note that some of these AOD observations sometimes pass the Version 2 cloud-screening algorithm and therefore reach Level 1.5. However, the Version 2 database quality control criteria require that a minimum of three AOD observations per day pass the temporal variability thresholds (AOD 1-min triplet range and daily time series checks for temporal spikes; Smirnov et al., 2000) to reach Level 2.

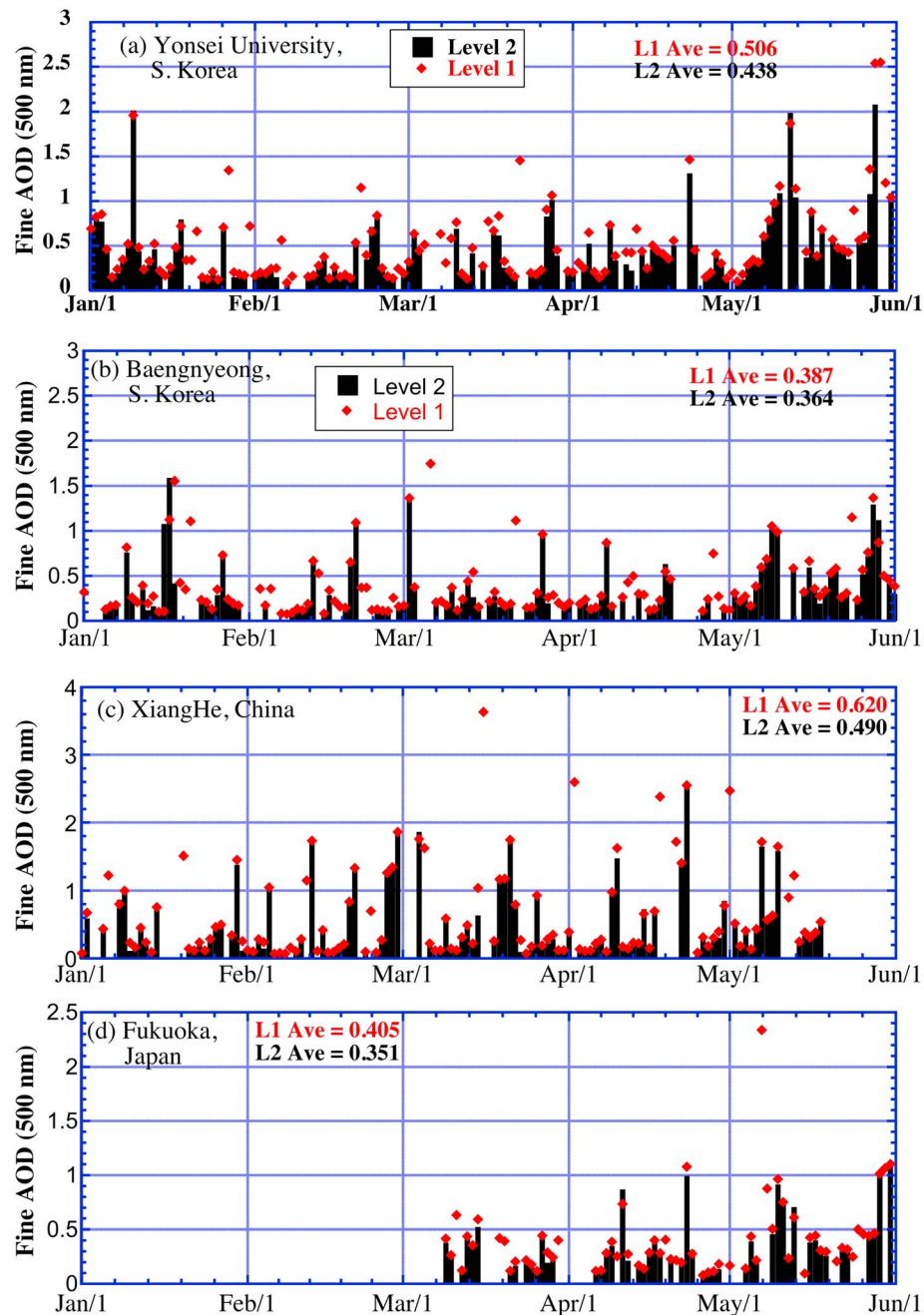


Figure 1. Time series of daily averages of fine mode AOD at 500 nm (Version 2, V2) retrieved from spectral deconvolution algorithm from 1 January to 1 June 2012 for Aerosol Robotic Network sites at (a) Yonsei University, South Korea, (b) Baengnyeong, South Korea, (c) XiangHe, China, and (d) Fukuoka, Japan. Note that days with only a red diamond (L1) and no black bar (L2) did not pass V2 Level 2 cloud screening. AOD = aerosol optical depth.

At all of these sites, many of the Level 2 screened high AOD fine mode dominated days comprised a significant percentage of the total number of days when AOD at 500 nm exceeded 1.0. For example, at the Xianghe, China site, 4 of the 5 days where daily average fine mode AOD at 500 nm exceeded 2.0 were cloud screened in Version 2 (see Figure 1c). The Ångström exponent (440–870 nm) for these four cloud-screened days ranged from 0.62 to 1.14 and the FMF of AOD at 500 nm from 0.62 to 0.97. This suggests that many major particulate air pollution events are often associated with extensive cloud cover. However, time interval averaging that yields similar L1 and L2 fine mode AOD values does not necessarily mean that some major aerosol events were not eliminated by cloud screening in the Version 2 data. For example at the Gwangju GIST site

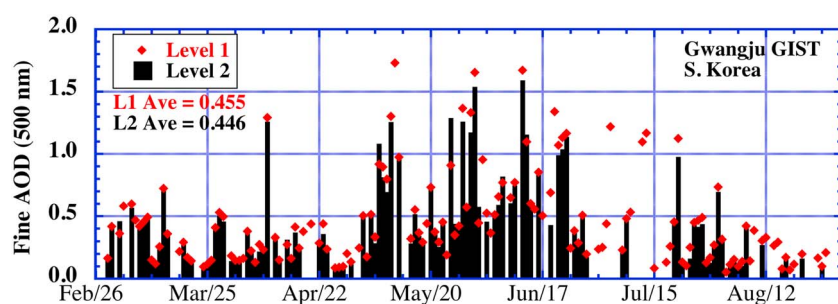


Figure 2. Similar to Figure 1 but the time series of daily averages of fine mode AOD at 500 nm (Version 2) retrieved from spectral deconvolution algorithm for the Aerosol Robotic Network site at Gwangju GIST, South Korea. Note that cloud screening at times removes both high and low AOD days (see, e.g., before and after 15 July), resulting in a similar time series average. AOD = aerosol optical depth.

(29 February to 27 August 2012) some high AOD events (>1) are eliminated by L2 cloud screening (see Figure 2). However, some low AOD fine mode events are also eliminated by cloud screening, when cirrus clouds occurred with an underlying low AOD layer (see, e.g., 15 July). As a result the ~ 6 -month mean AOD averages for this site are very similar (within ~ 0.01) for L1 and L2 even though several large fine mode AOD days were eliminated by the cloud screening.

Additionally, we attempt to determine how much influence the missing high AOD days in L2 have on the differences in time interval average values for one site. For the Yonsei site (Figure 3) we compare the L1 and L2 fine mode AOD data for only those days when both levels have a daily mean value. For January through May 2012, for this day-matched data set the fine mode AOD at 500 nm was 0.028 lower for cloud-screened data (L2) versus non-cloud screened (L1). However, the AOD was 0.068 lower in L2 than in L1 when all dates were averaged, including days when cloud screening eliminated days with high level pollution AOD (but very few observations). Therefore, for this site and time period $\sim 60\%$ of the higher fine mode AOD in the non-cloud-screened data ($100 \times (0.068 - 0.028) / 0.068$) is due to the cloud screening eliminating days of high aerosol loading events. The remaining increase in AOD in L1 for matched days is mainly due to high variability of AOD in the near vicinity of clouds that is eliminated by L2 screening (see Eck et al., 2014, for this phenomenon in the vicinity of cumulus clouds). High temporal variability of fine mode AOD near to clouds may be due to the turbulent and dynamic physical and chemical environment often associated with clouds, especially cumulus. The relative differences in extended time interval averages (months) for L1 versus L2 fine mode AOD for time matched days only versus all days vary widely between sites; for instance, time interval average differences for all days included are minor for the Gwangju GIST site (Figure 2), but large and significant differences are seen for the Xianghe site.

Now we examine a selected data example to compare the cloud screening of Version 3 with Version 2. The AERONET DRAGON_Korea_Univ site was located in central Seoul, and during the time period from 27 to 31 May 2012 there was a major aerosol event with fine mode AOD levels exceeding 1.0 at 500 nm throughout this 5-day period. Some of these days also had high cloud fraction as seen in MODIS Terra and Aqua images (see Figures 4b and 4c). The AERONET Version 2 automated cloud screening (Level 1.5 data) resulted in screening of all but one or two observations on the 3 days that had the highest AOD of this interval from 28 to 30 May (Figure 4a). Since these 3 days had less than the minimum number of AOD observations per

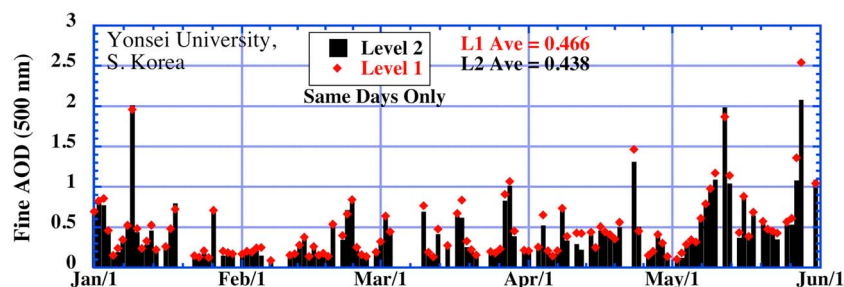


Figure 3. Similar to Figure 1 but the time series of daily averages of fine mode AOD at 500 nm (Version 2) retrieved from spectral deconvolution algorithm for the Aerosol Robotic Network site at Yonsei University, South Korea but only showing days that have passed L2 cloud screening. AOD = aerosol optical depth.

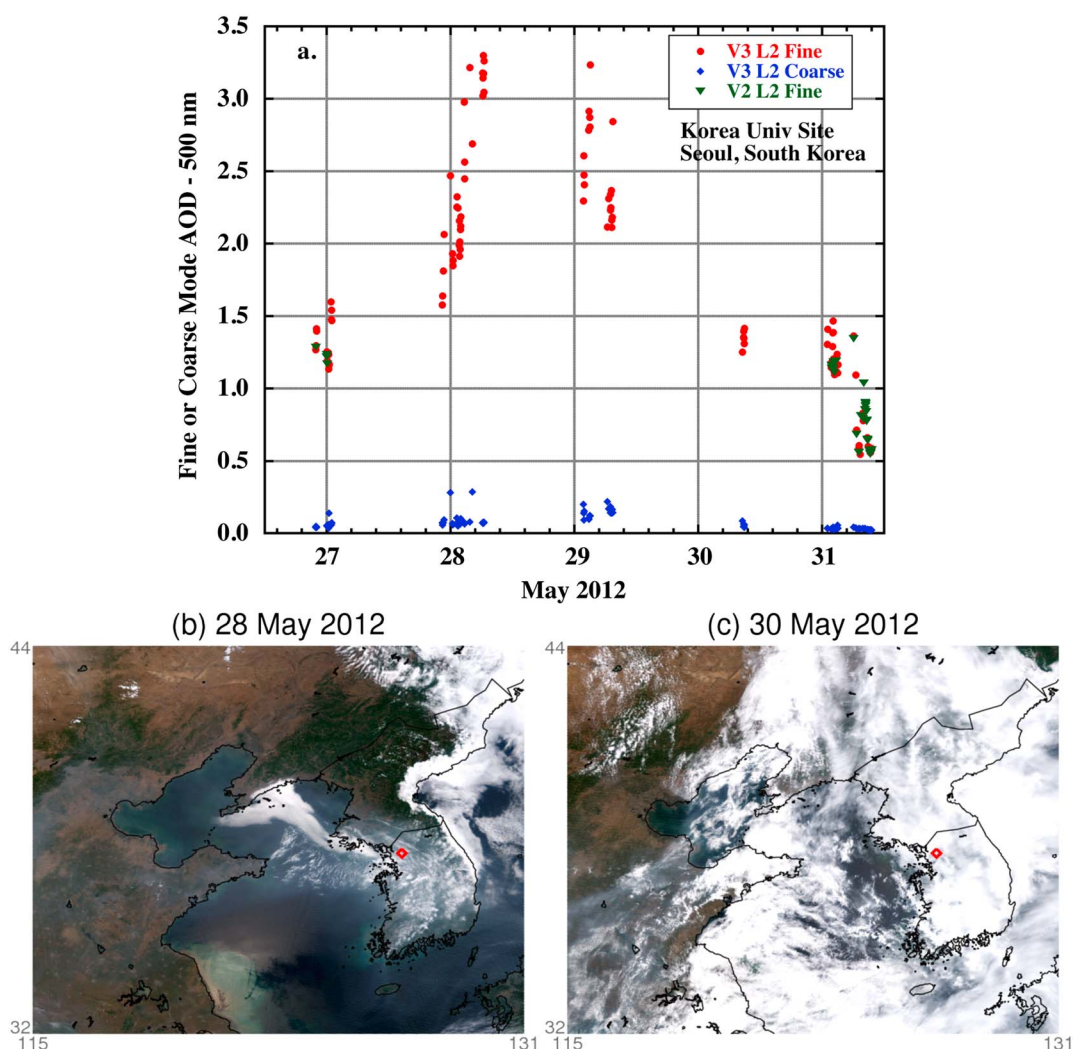


Figure 4. (a) The time series from 27 to 31 May 2012 of instantaneous values of fine mode AOD at 500 nm retrieved from spectral deconvolution algorithm for the Aerosol Robotic Network site at Korea University, in Seoul, South Korea, showing cloud-screened Version 2 data (green) plus Version 3 cloud-screened fine (red) and coarse (blue) mode AOD. Moderate Resolution Imaging Spectroradiometer Terra images for 28 and 30 May are shown in (b) and (c), with the Korea University site marked by a red diamond. AOD = aerosol optical depth.

day (three) required for Level 2, there were no AOD data for these 3 days in the Level 2 database. Similar cloud screening occurred for the Yonsei University site (see Figure 1a) on these same dates as both sites are located in Seoul, as well as similar time series for the other nine sites located in the greater Seoul region during this major pollution event. However, the new Version 3 cloud screening passed multiple AOD observations for all three of these days (ranging from 6 to 33 points per day; Figure 4), resulting in more complete monitoring of this major aerosol pollution event (average Ångström exponent [440–870 nm] of 1.21). This difference in cloud screening is largely due to the change in triplet variability tests (cf. section 2.1.1.). At the longer wavelengths the fine mode AOD decreases rapidly with increasing wavelength, while coarse mode AOD and/or cloud droplet optical depth is nearly constant with wavelength; therefore, the triplet variance at longer wavelengths is more attributable to supermicron particle/droplet variation (cloud or dust). In other words, the FMF of AOD decreases as wavelength increases, as shown in Eck et al. (2010). The average FMF of AOD at 500 nm was 0.95 over this 5-day interval, from V3 Level 2 daily average data as computed from SDA, therefore obviously a fine mode aerosol dominated event (as also suggested by the high Ångström exponent). Version 3 cloud screening also has a check for Ångström exponent (440–870 nm), and if it exceeds 1.0 for an instantaneous measurement, then even small numbers of such AOD observations per day are retained in Level 2 database. This case clearly illustrates the enhanced effectiveness of the Version 3 cloud screening

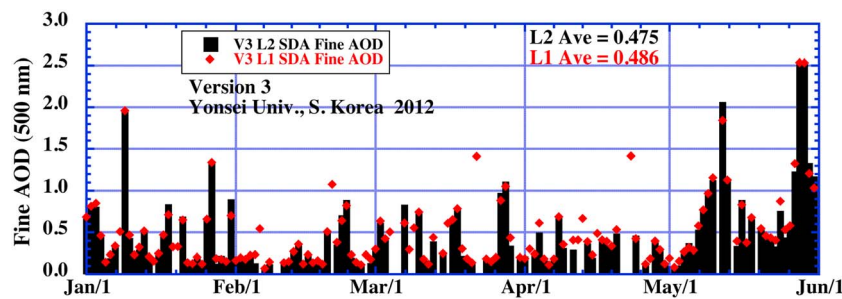


Figure 5. Similar to Figure 1a but the time series of daily averages of fine mode AOD at 500 nm retrieved from spectral deconvolution algorithm for the Aerosol Robotic Network site at Yonsei University, South Korea, but for Version 3 cloud and quality assurance screening. AOD = aerosol optical depth.

and QA algorithms in correctly identifying fine mode aerosol cases. Version 2 cloud screening clearly at times misidentified fine mode aerosol variability for cloud contamination, resulting in rejection of the data.

A comparison of cloud-screened versus non-cloud-screened daily average fine mode AOD from SDA for Version 3 data at the Yonsei University site is shown in Figure 5. This is the same site and time period as shown in Figure 1a (above) for the Version 2 data and can be compared for the differences in cloud screening in Versions 2 and 3. Note that some high AOD days that were cloud screened in Version 2 are not cloud screened in Version 3. Notably, high fine mode AOD days on 25 January and 28–29 May reach Level 2 in Version 3 but are screened from Level 2 data in Version 2. On the other hand, the high fine mode AOD day on day 114 (23 April) is screened from Version 3 as cloud, while these data pass the Version 2 cloud screening checks. Note that there is a cloud-screening check in Version 3 for cirrus that does not utilize temporal variance for cloud detection as in Version 2. Instead, it relies on independent measurements of sky radiance in the solar aureole as a means of identifying cirrus clouds. If the angular slope of the sky radiance is steep, there likely are cirrus cloud crystals present (due to very strong forward scattering) and there is a threshold on this angular dependence for determining cirrus presence. However, in this case differences in temporal variance checks (triplets and data spike filter) and differences in the thresholds of the number of observations per day resulted in elimination of the data in Version 3, while it was retained in Version 2. In fact, for this day there were 12 observed AOD spectra that passed the V3 temporal variance cloud screening checks but since the Ångström exponent was less than 1 (~ 0.8 – 0.93), this was below the minimum number of points (13) required for the day (minimum 10% of total possible measurements). Lidar data from nearby Seoul National University showed no directly overhead cirrus present at this time on this day. The 2 days where both Version 2 and Version 3 screen high AOD events as cloud (22 February and 22 March) seem to have cirrus cloud overlaying an aerosol layer and are screened from Level 2 in both Versions 2 and 3; therefore, the only way to detect these high fine mode AOD events when utilizing AERONET data is from SDA Level 1 (non-cloud-screened) retrievals.

It is noted that simulation studies of cirrus clouds overlying an aerosol layer (Smirnov et al., 2018) show that the SDA algorithm may underestimate the fine mode AOD by $\sim 5\%$ to $\sim 25\%$ (depending on cirrus crystal size, cirrus optical depth, and AOD magnitude). For cirrus crystal size similar to that retrieved by MODIS Collection 6 data for all latitudes, ~ 30 – 35 - μm effective radius (Yi et al., 2017), this study suggests that the SDA underestimate of fine mode AOD may be on the order of $\sim 10\%$ to 15% . Therefore, for these particular high fine mode AOD days with overlying cirrus at the Yonsei University site, the actual fine mode AOD may have been somewhat higher than the already high fine mode AOD retrieved by the SDA algorithm (SDA fine AOD[500 nm] > 1.1). Thus, the conclusions and main findings of this paper are unchanged even if the fine mode AOD estimated by SDA are lower than the actual values as suggested by the Smirnov et al. (2018) simulations. However, empirical evidence of this SDA underestimate of fine mode AOD as suggested by these simulations is often lacking and not provided by Smirnov et al. (2018). For example, time series of fine mode AOD on a day with moderate to high optical depth cirrus alternating with cloudless periods often do not show a decrease in fine AOD when the cirrus is overlying the aerosol layer compared to when cirrus is not partially obscuring the Sun.

The maximum AOD that can be measured by AERONET (and all Sun photometers) is ~ 7 for overhead Sun and $\text{AOD} \cdot m < 7$ (where m = optical air mass) for other SZAs. At AOD values higher than ~ 7 the Sun is no longer

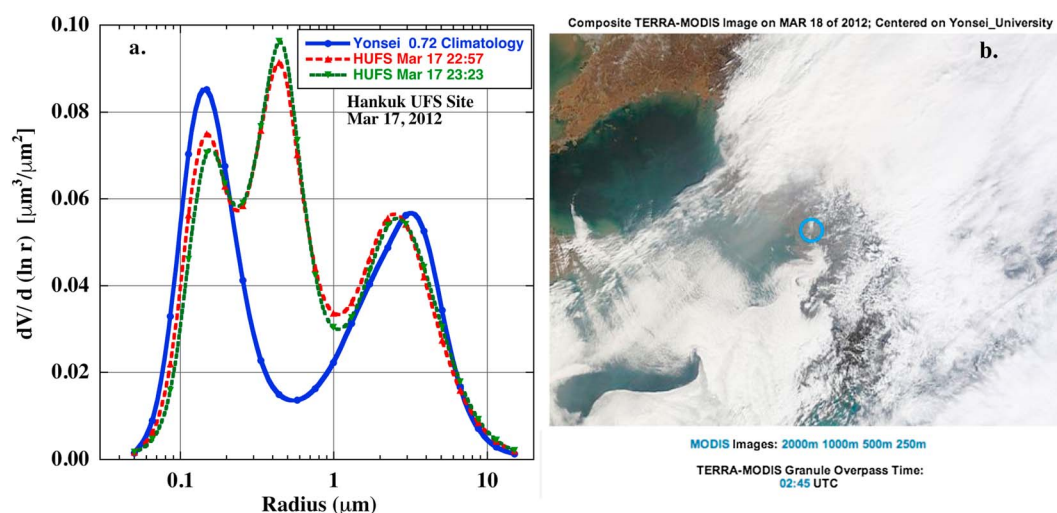


Figure 6. (a) Almucentar retrievals of aerosol size distributions from Aerosol Robotic Network measurements made at the Hankuk UFS site on 17 March 2012, as compared to climatological mean size distributions from the Yonsei University site utilizing 42 retrievals from March to May 2011 and 2012 with average fine mode fraction (440 nm) of 0.88 and AOD(440 nm) ranging from 0.6–0.8. (b) MODIS Terra image from about 4 hr after the Hankuk UFS retrievals shown in (a). The blue circle indicates the Yonsei University site location. MODIS = Moderate Resolution Imaging Spectroradiometer.

visible and significant diffuse radiation is present (direct beam signal nearly completely attenuated, see Sinyuk et al., 2012). In Version 3 very high AOD data are retained in the longer wavelengths (675 to 1,640 nm) if the Ångström exponent is sufficiently high (>1.2 for 675–1,020 nm or >1.3 for 870–1,020 nm) when the solar radiation at the ultraviolet and visible wavelengths is attenuated to levels below the instrument sensitivity. However, robust SDA retrievals require all wavelengths from 380 to 870 nm (five channels) be utilized as input: therefore, we do not analyze the impact of these particular extremely high AOD events in this paper. Additionally, AERONET measurements cannot detect AOD in the presence of moderate to thick clouds, including most cumulus clouds when COD exceeds 7. As a result there is a sampling bias from AERONET measurements (and satellite retrievals also) that results in a lack of characterization of AOD in major cloud systems with moderate to high COD. Additionally, AERONET does not attempt measurements during precipitation, since a wet sensor signal keeps the instrument in parked mode (looking down) to help protect the optical lenses from water and solute contamination. However, the data that we are analyzing here of fine mode AOD from SDA retrievals of L1 data provide better characterization of AOD in the near-cloud environment (as compared to cloud-screened data), or in cases where few small gaps in the clouds allow for very few direct Sun observations over the course of the day.

3.2. Aerosol Processing by Fog and/or Low-Altitude Layer Cloud

In this section we examine how cloud and/or fog processing of particles may significantly modify the particle size distribution in the fine mode. In Figure 6 the South Korean Hankuk University of Foreign Studies site (Hankuk_UFS) almucentar volume size distribution retrievals from 17 March 2012 are compared with the spring season average size distribution at the Yonsei University site for the months of March through May of both 2011 and 2012. These two sites are located in the same region, ~38 km apart. On 17 March 2012 at the Hankuk_UFS site during the time of these almucentar retrievals the AOD at 440 nm was 1.03 and the Ångström exponent (440–870 nm) was ~0.96. The spring season mean at the Yonsei University site was computed as the average of 42 Level 2 almucentar retrievals with a mean FMF of AOD of 0.88 at 440 nm with AOD at 440 nm ranging from 0.6 to 0.8. The MODIS Terra image from ~4 hr after the time of the retrievals shows extensive cloud cover plus layer cloud over the Yellow Sea that may be fog. Both the smaller radius fine mode and the coarse mode size distribution of this case at Hankuk_UFS are very similar to the Yonsei climatological size distributions. The significant difference is the presence of the middle submicron-sized mode with radius ~0.4–0.5 μm in the Hankuk_UFS retrievals. It is noted that three other sites (Yonsei University, DRAGON_NIER, and Anmyon) had almucentar retrievals on 18 March 2012 (about 8–9 hr later) that also had a submicron middle mode. Additionally, the Anmyon site was 126 km from Yonsei in

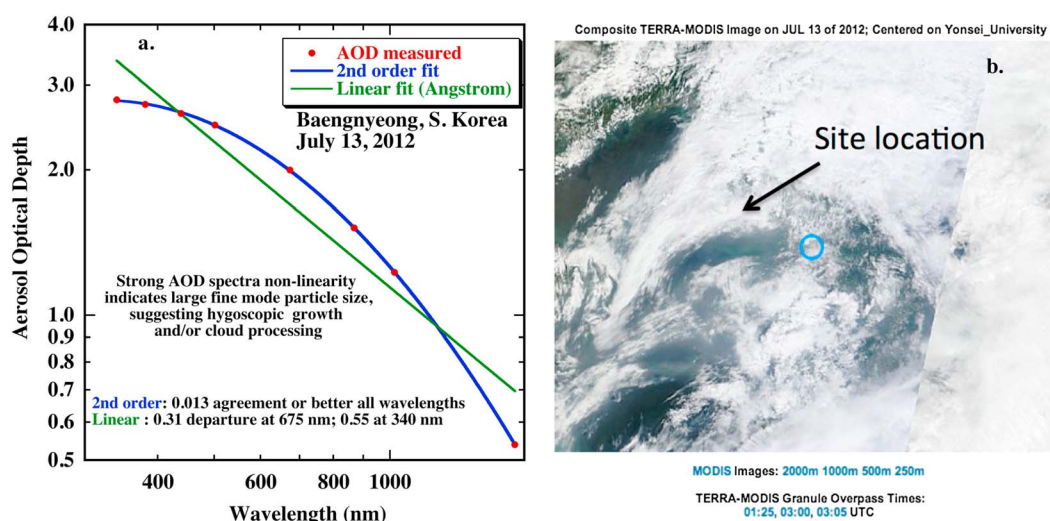


Figure 7. (a.) Spectral AOD measurements at the Baengnyeong, South Korea site, on 13 July 2012, with linear and second-order regressions in logarithmic coordinates. (b.) MODIS Terra image from about 1 hr before the Baengnyeong AOD spectra shown in (a). The blue circle indicates the Yonsei University site location and the arrow shows the Baengnyeong site location. AOD = aerosol optical depth; MODIS = Moderate Resolution Imaging Spectroradiometer; UTC = universal time coordinated.

central Seoul, thus suggesting widespread presence of this middle mode particle size on this day. Both Eck et al. (2012) and Li et al. (2014) have shown this mode to be associated with cloud or fog processed aerosols, and Li et al. (2014) determined that this cloud processed or residual aerosol mode was typically best fit by a size distribution with 0.44- μm median radius and width defined by geometric standard deviation of 1.49. These middle sized aerosol particles have also been measured in situ by Dall'Osto et al. (2009) associated with fog occurrence. Some chemical species of this middle mode, such as hydroxymethane sulfonate, are only formed in the aqueous phase (Munger et al., 1986; Whiteaker & Prather, 2003). This case is shown as an example of observed aerosol modification by cloud/fog in this region as part of the overall greater issue of spectral AOD observations associated with aerosol-cloud interactions (see Figure 7 below and associated text).

3.3. Observations of Near-Cloud AOD Spectra

Since the AOD spectra are the key to separating fine versus coarse modes in the SDA algorithm, we examine the spectra of a single case (and how it relates to possible middle mode aerosol mentioned above) and also the parameter $da/d\ln\lambda$ (α') that varies as a function of fine mode particle size (Eck et al., 2001; Reid et al., 1999) and is a key input to SDA. A single day case study at the Baengnyeong Island, South Korea site, on 13 July 2012 is shown in Figure 7. There was only one observation of AOD made all day at the site due to the extensive cloud cover (see MODIS Terra image in the figure), and the fine mode AOD retrieved from SDA was very high at 2.40 at 500 nm, with FMF of 0.97. This measured AOD spectrum suggests large fine mode particle size due to the strong spectral nonlinearity of the AOD in logarithmic space with $\alpha' = 1.30$ (Eck et al., 1999, 2001; Reid et al., 1999). High values of spectral nonlinearity can only occur when large accumulation mode particles dominate as shown from Mie calculations in Eck et al. (1999, 2001). Figure 1 of O'Neill et al. (2001) indicates that these optical phenomena correspond to a situation where the spectral curvature is at or near the spectral curvature of the anomalous diffraction peak of the extinction efficiency: this appears as a broad peak in α'_f (the fine mode value of α' when the FMF is large) at smaller, subunity values of α'_f (corresponding precisely to large fine mode particles). This large fine mode particle size may be due in part to particle humidification growth in/near clouds and/or cloud processing of aerosol particles.

Mie calculations were made for a cloud processed aerosol mode as defined by Li et al. (2014), where volume median radius is 0.44 μm and geometric standard deviation is 1.49, which results in α' of 1.81 and Ångström exponent (440–870 nm) of 0.26. The values of 1.45 and 0.01 that we assumed for the real and imaginary refractive indices are typical AERONET retrieval values for summertime pollution in eastern China. Additional Mie calculations were performed for humidified aerosol where the assumed volume median radius was 0.25 μm and the assumed geometric standard deviation was 1.49 (typical summer values for

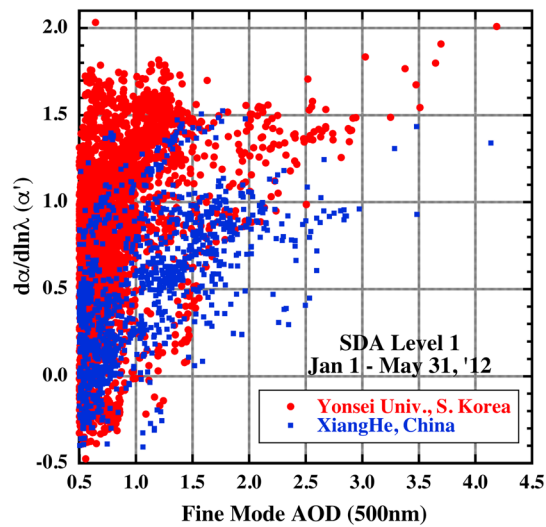


Figure 8. Computations of the parameter $d\alpha/d\ln\lambda$ (α') from instantaneous measurements of AOD made at the Yonsei University and XiangHe Aerosol Robotic Network sites from 1 January to 31 May 2012. This parameter is partly indicative of fine mode particle size but also affected by coarse mode fraction of AOD. AOD = aerosol optical depth.

high AOD fine mode aerosol in eastern China), and where the resulting α' was 1.77 and the Ångström exponent (440–870 nm) was 1.52. Then, AOD spectra were computed from Mie code calculations for a combined 50% cloud processed mode (0.44- μm volume radius) and 50% humidified mode (0.25 μm) resulting in α' of 1.41 and Ångström exponent (440–870 nm) of 0.83. This case agrees closely with the measured derivatives from the AOD spectra of α' of 1.30 and Ångström exponent (440–870 nm) of 0.80. Of course, there is no way to know from available measurements if both of these assumed fine modes comprised 50% of the total AOD, and the humidified mode may have had smaller or larger fine particles than assumed here. However, these Mie calculations are presented as a potential (perhaps likely) explanation of humidified plus cloud processed fine particles resulting in the observed AOD spectra.

Additionally, the satellite imagery showing extensive cloud cover along with the sparseness of AERONET measurements of AOD (also due to clouds) is consistent with the measured AOD spectra that can only be explained by large fine mode particles likely resulting from both cloud processing and aerosol humidification. This AOD spectra observation on this day at Baengnyeong was eliminated by cloud screening by both Version 2 and Version 3 cloud screening algorithms; therefore, the only way to detect this fine mode event

with AERONET was from Level 1 data utilizing SDA. Note that of the eight other AERONET sites in South Korea on this date (13 July 2012), three sites had no Level 1 data, while five sites had Level 1 SDA fine mode AOD(500 nm) ranging from 0.88 to 1.30, and only one site had three points that would pass cloud screening to Level 2 in Version 2. This sparseness of direct Sun observations combined with high fine mode AOD again shows that high pollution AOD events are often associated with extensive clouds and that these events are difficult to detect from remote sensing measurements.

The α' parameter (indicative of fine mode particle size) shows a strong increasing tendency as AOD increases, at both the XiangHe and Yonsei sites for January through May 2012 (Figure 8). This trend in α' is consistent with increasing fine mode radius as AOD increases (Eck et al., 2003, 2010). This assertion is effectively a corollary of the algorithm reported in O'Neill et al. (2005, corrected in O'Neill et al., 2008) where it was demonstrated that the fine mode effective radius, in the presence of fixed refractive index (fixed aerosol type), was a strong function of a ratio involving α'_f over α_f . Increases in particle radius as AOD increases may result from a combination of several physical factors: increased coagulation rates at high aerosol concentrations, humidification (sometimes in high RH cloudy environments), and also cloud processing of particles. Additionally, note that the values of α' are higher for Yonsei than for XiangHe at the same AOD levels, possibly due to further aging and processing of fine mode aerosol as it is transported from China to Korea (potentially resulting in larger fine mode particles in Korea). However, much of the difference in α' is due to the frequently higher coarse mode fractions in China due to closer proximity to arid lands (dust sources) and also possibly more coarse mode fly ash associated with coal combustion and combustion of other fuels in China (Yang et al., 2009). For all observations in this time interval where AOD at 500 nm exceeded 1, the average FMF of AOD at 500 nm for the Yonsei University site was 0.92 versus 0.84 for the XiangHe site; thus, on average significantly higher coarse mode was present at the site in China. These coarse mode particles may diminish from gravitational settling in transport to South Korea. Also, the coarse mode particles associated with fuel combustion are not emitted as much in South Korea as compared to China, due to the number and type of sources and also emission control differences.

3.4. Comparison of MODIS Satellite Detection of Fine Mode AOD Events to AERONET

In this section we examine the ability of MODIS satellite algorithms to detect high-magnitude AOD events for two selected sites in the region. The daily averages of AERONET L1 fine mode 550 nm AOD were compared to L2 and to daily spatial averages of MODIS retrievals of total AOD at the XiangHe site from 1 January to 18 May 2012. The satellite daily data are computed by averaging retrievals over a 30-km

radius for DT and DB and 61- by 61-km square for MAIAC. It is noted that AERONET has much higher sampling frequency than satellite, that is, 15 min or less from SZA of 82° in the morning and to the same SZA in the evening, while MODIS has only two overpasses per day. However, the spatial coverage of MODIS, as selected for this comparison study, is significantly greater than a single AERONET site, partially compensating for lesser temporal coverage.

The time series of SDA L1 Fine mode AOD compared to satellite retrievals of AOD by the MODIS DT algorithm shows that this algorithm screens many high AOD (>0.8 at 550 nm) events at XiangHe in 2012. Figures 9a–9c show the daily mean AOD(550 nm) time series at XiangHe for SDA L1 versus MODIS retrievals for the Collection 6 database DT, DB, and MAIAC algorithms respectively. In Table 1, the AERONET and MODIS data sets are compared for detection of high AOD events, with the threshold of AOD(550 nm) > 0.8 . Only one MODIS overpass retrieval having AOD(550 nm) > 0.8 was required to meet the high AOD threshold for comparison purposes, while for AERONET the daily averages are required to exceed the threshold. A comparison of the AERONET SDA L1 versus L2 shows that the AERONET Version 2 cloud screening results in missing 38% of the high AOD days. Both the DB and MAIAC algorithms also had no AOD retrievals on a similar number of these days, 44% and 41% respectively. In DB, based on this analysis and others, improved smoke detection tests have recently been developed to identify thick and/or spatially variable smoke events such as these, which are screened out by the C6 algorithm version. The upcoming MODIS C6.1 DB data set is therefore expected to suffer from less of a sampling bias in these conditions than C6. The DT algorithm retrieves AOD on only 3 days from day 1 to 80 (1 January to 20 March) in 2012. This is the main reason that the DT algorithm misses 75% of the high fine mode AOD events that are identified by SDA in Level 1. However, it is noted that for some days there is cloud cover present during the Terra and Aqua overpasses yet not cloud at some other time periods when AERONET is sampling the AOD. Additionally, since all three algorithms utilize input data from the same satellite measurements, the differences between retrievals shown here seem likely to be due in large part to differences in cloud screening.

All three MODIS AOD retrieval algorithms also added days of high AOD that are missed by AERONET L1 in SDA. For some of the highest AOD days that DB made a retrieval yet SDA L1 did not at XiangHe, the Beijing AERONET site (~60 km to the WNW of XiangHe) measured AOD > 2 , suggesting that clouds covered the XiangHe site for the entire day yet did not extend westward all the way to Beijing. Therefore, at least some (if not most) of the added days by the MODIS retrievals were due to greater spatial sampling by the satellite, while the other possibility is potential cloud contamination of the MODIS retrievals.

Similar comparisons for the Yonsei University site in Seoul showed that all three satellite retrieval algorithms missed most days of high fine mode AOD identified by the Level 1 SDA retrievals from AERONET, missing 65%, 82%, and 71% of these days for DT, DB, and MAIAC respectively. However, it is noted that Seoul is flanked in many directions by low-altitude mountains that nonetheless extend in altitude above a fraction of the aerosol layer. Therefore, spatial averages of satellite retrievals of AOD centered on the Yonsei site include lower AOD over the mountains averaged with higher AOD over the lowlands (where the Yonsei University site is located). Therefore, it is expected that the spatial average satellite retrievals at Yonsei University (in Seoul), which average both samples of lower AOD over the mountains and higher AOD in the lowlands, would be biased low versus the point AERONET measurement at this lowland site.

3.5. DA Model Identification of Major Fine Mode AOD Events

Two DA models (NAAPS and MERRAero) both showed underestimation of Fine Mode AOD at 550 nm compared to L1 fine mode AOD from SDA, with greater underestimation for the higher AOD cases that were eliminated by L2 AERONET cloud screening (Version 2 SDA; Figure 10). Note that both the NAAPS version shown here and the MERRAero model did not assimilate AERONET data, while the more recent MERRA-2 reanalysis does (Buchard et al., 2017; Randles et al., 2017). Data temporal collocation is important in comparison of aerosol data sets (Schutgens et al., 2016). Therefore, we have compared only daytime (sunlit hours when AERONET measurements are possible) to daytime hours of the NAAPS and MERRAero DA model results. However, close time matching has not been employed with either the model or satellite measurements. Therefore, more frequent sampling by AERONET (15- or 3-min measurement interval, depending on instrument mode) from SZA of 82° in the morning to 82° in the evening give AERONET a much higher probability of measuring AOD in cloudy conditions. Figure 10 shows these comparisons, additionally showing the time series of Collection 5 MODIS DT retrievals of AOD since C5 is the satellite data assimilated into the models. The

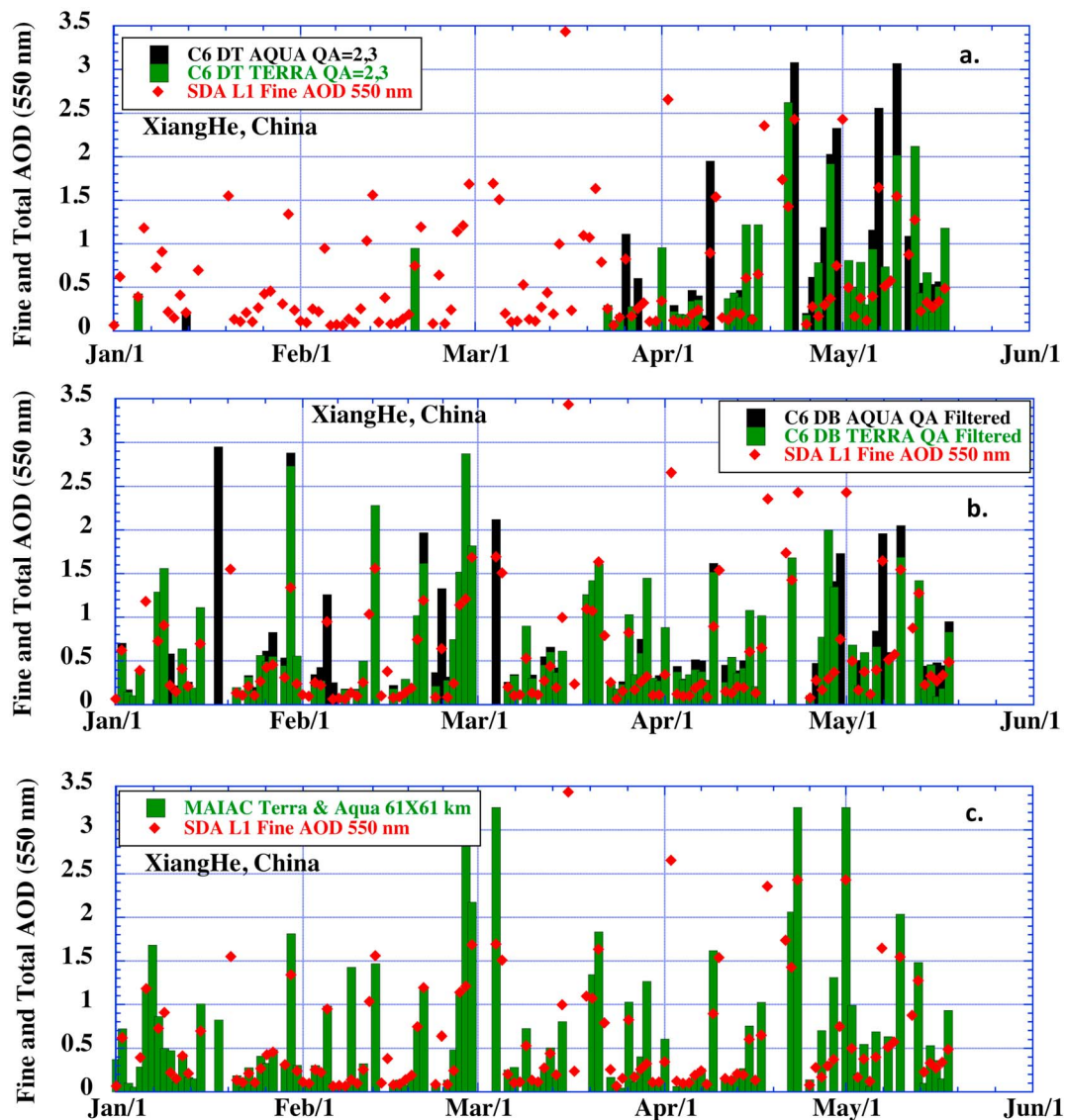


Figure 9. Time series of daily averages of Aerosol Robotic Network Level 1 fine mode AOD at 550 nm (Version 2) retrieved from spectral deconvolution algorithm from 1 January to 1 June 2012 for the Aerosol Robotic Network site at XiangHe, China, compared to MODIS Collection 6 satellite retrievals of total AOD from (a) Dark Target, (b) Deep Blue, and (c) MAIAC algorithms. AOD = aerosol optical depth; MODIS = Moderate Resolution Imaging Spectroradiometer; MAIAC = Multi-Angle Implementation of Atmospheric Correction; QA = quality assurance.

lack of DT retrievals of high AOD days from day of year from 1 to ~85 clearly results in a handicap to the assimilation models. This suggests a combination of factors in the DA models pertaining to underestimation of high AOD events, including possible underestimation of aerosol source functions, lack of satellite retrievals for some high AOD events, and possible insufficient humidification growth in

Table 1
XiangHe, China, 1 January to 18 May 2012 SDA Fine Mode Daily Averages MODIS-Terra + Aqua

Retrieval	SDA fine L1	SDA fine L2	Dark Target	Deep Blue	MAIAC
Days ^a	32	22	12 (+8 dust ^b)	27 (+8 dust ^b)	25 (+4 dust ^b)
Days missed versus L1 fine mode	N/A	12	24	14	13
% Missed versus L1 (fine AOD days)		38%	75%	44%	41%
% Added days-nondust days		6% (2 days)	12% (4 days)	28% (9 days)	19% (6 days)

Note. Days with AOD(550 nm) > 0.8.

^aDB and DT spatial aggregation is 30-km radius, and MAIAC is 61 × 61 km. ^bDust days identified as >50% coarse mode in SDA L2, and fine AOD < 0.8 in L1 and L2.

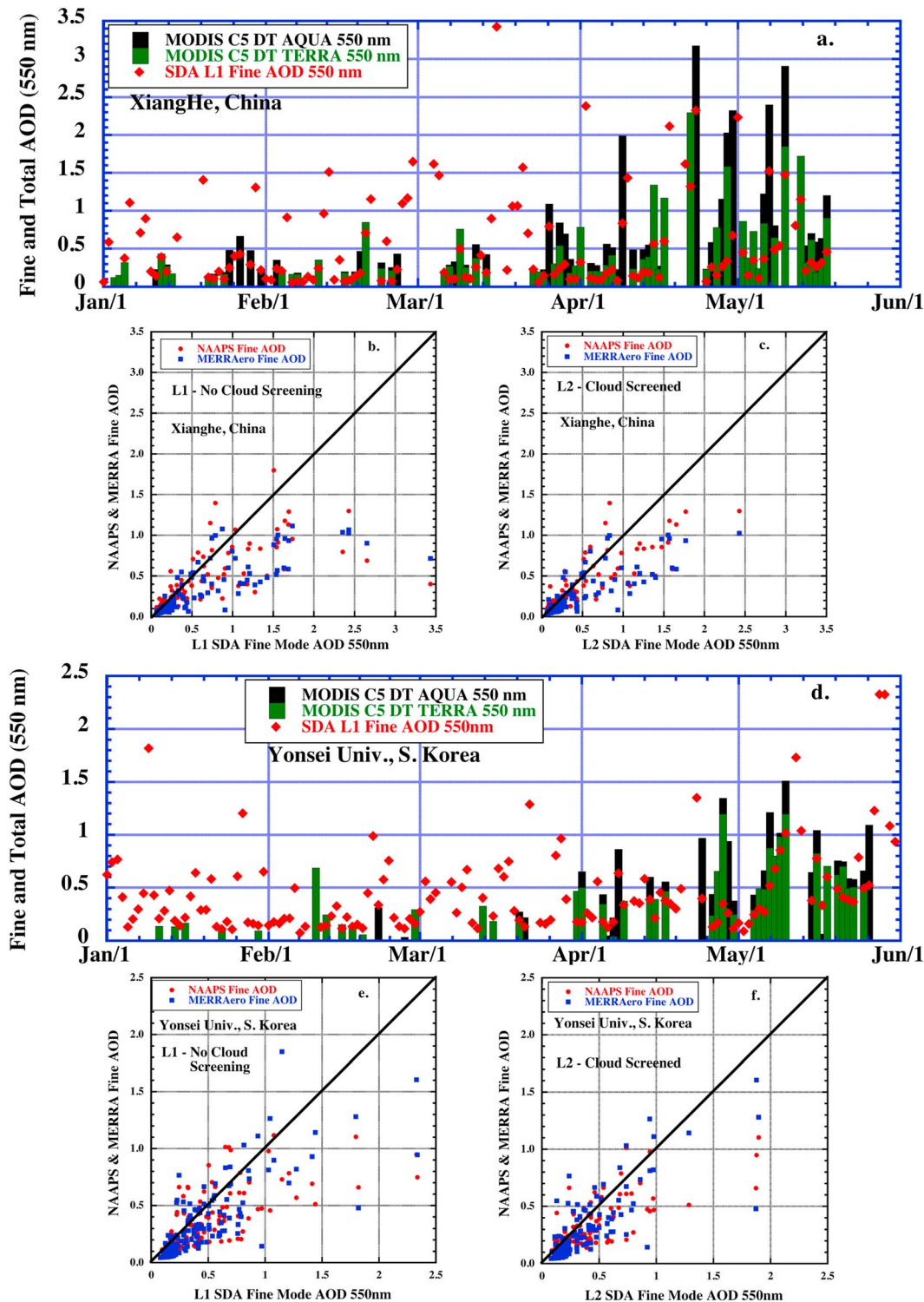


Figure 10. (a) Time series of daily averages of Aerosol Robotic Network (AERONET) Level 1 fine mode AOD at 550 nm (Version 2) retrieved from spectral deconvolution algorithm (SDA) from 1 January to 1 June 2012 for the AERONET site at XiangHe, China compared to MODIS collection 5 satellite retrievals of total AOD from the Dark Target algorithm. (b) Scatterplot of NAAPS and MERRAero modeled daytime average fine mode AOD compared to AERONET L1 fine mode AOD daily averages. (c) Same as (b) but for cloud-screened L2 fine mode AOD from SDA. (d) Time series of daily averages of AERONET Level 1 fine mode AOD at 550 nm (Version 2) retrieved from SDA from 1 January to 1 June 2012 for the AERONET site at Yonsei University compared to MODIS Collection 5 satellite retrievals of total AOD from the Dark Target algorithm. (e) Scatterplot of NAAPS and MERRAero modeled daytime average fine mode AOD compared to AERONET L1 fine mode AOD daily averages. (f) Same as plot (e) but for cloud-screened L2 fine mode AOD from SDA. AOD = aerosol optical depth; MODIS = Moderate Resolution Imaging Spectroradiometer; DT = Dark Target; NAAPS = Navy Aerosol Analysis and Prediction System; MERRA = Modern-Era Retrospective Analysis for Research and Applications.

near-cloud environments. MERRAero does not include cloud processing of aerosols in the Goddard Chemistry, Aerosol, Radiation and Transport Model aerosol microphysical model utilized.

Rubin et al. (2017) found that assimilation of AERONET observations of AOD in addition to MODIS data into an advanced ensemble assimilation of the NAAPS model resulted in increased forecasting skill for high AOD (>1) events with improvements in temporal variability in regions such as India and East Asia. The recent MERRA-2 reanalysis also adds assimilation of AOD observations from AERONET (Randles et al., 2017) and similarly also shows improved identification of high AOD events in eastern China (Buchard et al., 2017). In both the Rubin et al. (2017) NAAPS study and the Randles et al. (2017) MERRA-2 study the AERONET Version 2 Level 2 total AOD data were assimilated into the models. The MODIS Collection 5 AOD were also utilized or assimilated in both studies.

3.6. Climatological Analysis of AERONET Fine Mode AOD

Comparisons utilizing AERONET multiyear cloud-screened versus non-cloud-screened fine mode AOD were performed for selected sites that had at least 5 years of observations in all months. The comparisons, which included the analysis of monthly mean seasonal dynamics for this particular aerosol optical property, permitted a climatological-scale analysis. AERONET data from the sites of Yonsei University (6 years data) and Anmyon (5- to 7-year data varying by month), both in South Korea and also XiangHe, China (11 years data), are included in this section.

First, we examine how many days of data at selected high fine mode AOD thresholds are eliminated by the L2 cloud screening, in both Versions 2 and 3 of the AERONET database. In Table 2 (Version 2) and Table 3 (Version 3) we show the numbers of days of fine mode AOD data in L1 and L2 and their absolute and relative differences in number of days for various thresholds of minimum AOD levels. For the XiangHe site in Version 2, Table 2 shows that 32% of the data with daily mean AOD > 1 were screened at L2, while 46% were screened by L2 at AOD > 2 and 64% screened for days with average AOD > 3 . Note that for the XiangHe site the annual average Version 2 Level 2 total AOD at 500 nm is very high at 0.76 with monthly means for all summer months (June–August) ranging from 0.95 to 1.19. However, in Version 3 for the XiangHe site there were significantly fewer days eliminated by L2 cloud screening than in Version 2. For days with AOD > 2 at 500 nm the V3 cloud screening eliminated 17% of the days, while V2 screened 46% of the days for the same AOD threshold. Clearly the new Version 3 cloud screening and QA allows many more days of data with high levels of fine mode AOD to be analyzed. Similarly, for the Yonsei University site, for days with daily mean fine AOD > 1 at 500 nm, the V2 cloud screening eliminated 40% of the days while V3 cloud screening eliminated significantly fewer days at 15%.

Comparisons of frequency histograms of days that were eliminated by L2 cloud screening (without an AOD threshold) for both Versions 2 and 3 are shown in Figure 11. These eliminated days are the ones that exist in L1 data but are screened by L2 and are designated as L0 in Arola et al. (2017). The bin width is 0.1 AOD for the daily average fine mode L0 data. For the Yonsei University site there were significantly fewer days eliminated by the V3 cloud screening and QA than the V2 screening at all AOD levels. For the XiangHe site there were significantly fewer days of data eliminated by V3 when fine AOD was greater than 1 at 500 nm. Even though the difference in number of days between V3 and V2 is relatively large for low AOD at XiangHe, there is a relatively small percentage difference ($\sim 3\%$, for AOD < 0.5) of the ratio of eliminated days (L0) to total L1 days. The slightly greater elimination of low AOD days by V3 at this site is likely due in large part to the cirrus cloud screening check that utilizes the sky radiances in the solar aureole in V3.

In additional climatological data analysis, the L1 non-cloud-screened fine mode AOD (500 nm) increases as the total number of hours of data per day of cloud-screened L2 fine mode AOD observations decreases. This occurred for both the XiangHe, China, and Anmyon, South Korea sites, in both winter and spring (Figure 12.). These relationships suggest that higher fine mode AOD occurs when cloud cover increases, since missing hours of data are primarily due to greater cloud cover (and/or greater temporal variability of AOD that sometimes occurs in the near vicinity of clouds (Eck et al., 2014)). Greater cloud amount may be increasing fine mode AOD through humidification (since more clouds form when RH increases), cloud processing of existing particles, and/or new particle formation. Additionally, it is possible that higher fine mode AOD may contribute somewhat to increasing cloud amount due to reduced or delayed precipitation (cloud lifetime effect) or other aerosol-cloud feedbacks. Another factor that needs to be considered is that the AOD

Table 2

In AERONET Version 2 Data the Difference in Number of Days of Daily Average Fine Mode AOD (500 nm) in Level 1 (non-cloud screened) Versus Level 2 (Cloud Screened) for Different Lower Limits of AOD

Site name	Days of L1	Days of L2	Days L1-L2	% difference	AOD lower limit
XiangHe	3,672	3,058	614	17%	0
XiangHe	900	613	287	32%	1
XiangHe	280	150	130	46%	2
XiangHe	81	29	52	64%	3
XiangHe	25	5	20	80%	4
Yonsei University	1,744	1,381	363	21%	0
Yonsei University	167	101	66	40%	1
Yonsei University	14	5	9	64%	2

Note. Climatological data sets.

spatial and temporal variance tends to increase as AOD increases thus possibly resulting in erroneous screening of high fine mode AOD as clouds in some cases. Furthermore, meteorological covariation is likely a factor since many cloud-free days in this region occur with high atmospheric pressure systems that come from Siberia. The Siberian region has fewer aerosol sources (except when forest fires are occurring), and thus, AODs tend to be smaller. Also, high-pressure systems associated with the flow from the north have subsiding air that suppresses convection and cloud formation. Another factor that needs to be considered is that for both L1 and L2 data on very high fine mode AOD days ($AOD \sim >2$) only midday observations may exist due to full attenuation of the AOD signal for shorter wavelengths at large optical air mass (atmospheric path length).

The annual cycle of monthly mean fine mode AOD (500 nm) climatology using Version 2 data for both the Anmyon, South Korea site, and the XiangHe, China site, show ~ 10 – 15% higher AOD for L1 non-cloud-screened data as compared to L2 cloud-screened data (see Figures 13a and 13b) for most months due to cloud screening of some high AOD cases and also due to elimination of high-frequency AOD variability in the vicinity of cumulus clouds, which also tends to have higher AOD (Eck et al., 2014). Similar large differences in climatological L1 and L2 fine mode AOD (Version 2) in Asia were also found by Arola et al. (2017), who identified that this region globally had the largest relative increases compared to all other regions. Note that for both sites the monthly mean fine mode midvisible AOD (500 nm) increased dramatically from May to June, close to doubling at both Anmyon and XiangHe. June peaks in AOD in East Asia have been previously noted (Eck et al., 2005; Kim et al., 2007; Koo, 2008); however, the increase in total AOD from May to June is less of a jump than for fine mode AOD due to increased coarse mode AOD in spring months in the region. The dramatic increases in fine mode AOD are coincident with multiyear average increases in cloud fraction and RH from May to June and also with reduction in wind speed from May to June (Figure 13c). These meteorological factors are all consistent with increases in fine mode AOD, through particle humidification and growth, cloud processing and more rapid rates of new particle formation in clouds, as well as greater buildup of pollutants during

Table 3

In AERONET Version 3 Data the Difference in Number of Days of Daily Average Fine Mode AOD (500 nm) in Level 1 (Non-Cloud Screened) Versus Level 2 (Cloud Screened) for Different Lower Limits of AOD

Site name	Days of L1	Days of L2	Days L1-L2	% difference	AOD lower limit
XiangHe	3,673	3,183	490	13%	0
XiangHe	886	754	132	15%	1
XiangHe	273	226	47	17%	2
XiangHe	79	61	18	23%	3
XiangHe	23	17	6	26%	4
Yonsei University	1,741	1,519	222	13%	0
Yonsei University	164	140	24	15%	1
Yonsei University	14	10	4	29%	2

Note. Climatological data sets.

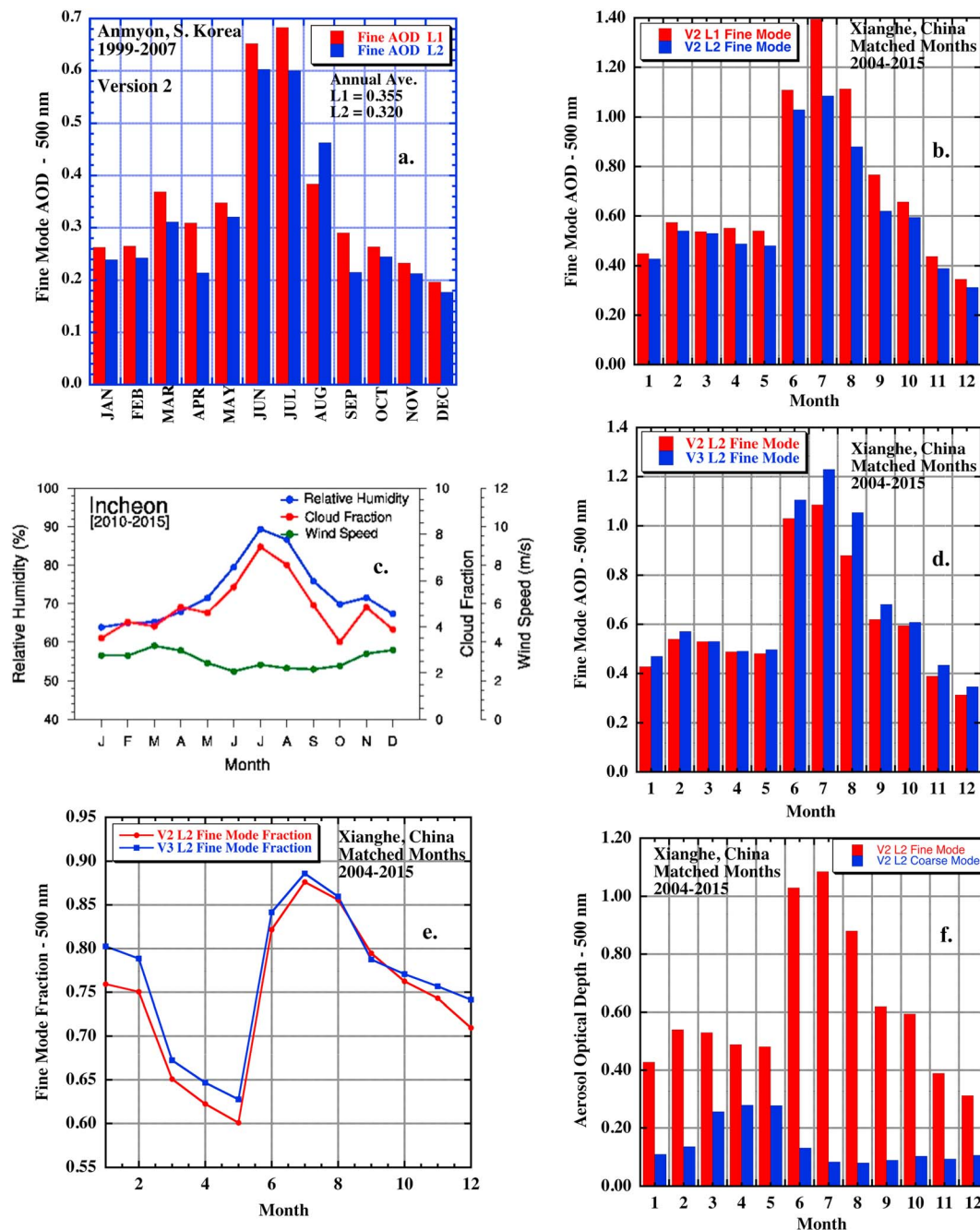


Figure 13. (a.) Multiyear monthly mean fine mode AOD (500 nm; Version 2) from spectral deconvolution algorithm (SDA), comparing cloud-screened (L2) to non-cloud-screened (L1) data for the Anmyon site in South Korea. (b.) Same as in (a) but for the climatological means at the Xianghe site in China. (c.) Multiyear averages of cloud fraction, relative humidity, and wind speed at the Incheon, South Korea site, ~110 km north of the Anmyon site. (d.) Multiyear monthly mean fine mode AOD (500 nm) from SDA, comparing cloud-screened (L2) data from Version 2 to the newer Version 3 for the Xianghe site in China. (e.) Monthly means of the fine mode fraction of AOD (500 nm) comparing results from Version 2 to Version 3. (f.) Multiyear monthly mean fine mode and coarse mode AOD (500 nm) from SDA, from Version 2 cloud-screened (L2) data for the Xianghe site in China. AOD = aerosol optical depth.

A comparison of the monthly mean fine mode AOD climatology for the XiangHe site between Versions 2 and 3 for matched months to the data shown in Figure 13b is shown in Figure 13d. The Versions 2 and 3 monthly means are nearly equal for April and May; however, most other months show higher fine mode AOD in Version 3. The differences in monthly mean AOD range from near 0 to ~0.035 from January to May; however, for the three summer months of June–August the Version 3 fine mode AOD at 500 nm is greater than Version

2 by ~ 0.075 , 0.133 and ~ 0.162 , respectively. The differences in AOD between the two versions are much greater in the summer months when cloud fraction is the highest, therefore suggesting (as also shown in Figure 5 and Tables 2 and 3) that Version 3 screens fewer high AOD fine mode aerosol events than Version 2. Also note that the monthly mean FMFs of AOD at 500 nm are similar between Versions 2 and 3 (Figure 13e), in all months even in spring when desert dust is more prevalent (Figure 13f). However, this paper focuses primarily on the fine mode AOD and the differences that occur between Level 1 and Level 2 data and also Versions 2 and 3 of the AERONET database. The differences in coarse mode AOD for sites that are dominated by coarse mode AOD or have mixtures of fine and coarse mode will be examined in more detail in future publications.

4. Summary and Conclusions

The occurrence of events with high fine mode AOD often associated with high cloud fraction in East Asia (Korea and upwind NE China) was examined utilizing AERONET and satellite retrievals. Analyses were focused primarily on AERONET data and included comparisons of direct Sun measured AOD from the algorithms utilized in Version 2 to the newly released Version 3 database that have significant differences in cloud screening, primarily based on temporal variance of AOD. While there are a number of cloud screening differences between V2 and V3, one of the most important differences is that temporal variance filtering is relegated to the longer, more coarse mode dependent, wavelengths in V3. It is emphasized that the differences in AOD between V2 and V3 cloud-screened data observed in this highly polluted, high AOD East Asia region may differ significantly from other regions on Earth.

1. Major aerosol pollution transport events with very high fine mode AOD (>1.0 in midvisible) in China/Korea/Japan were often observed to be associated with extensive cloud cover. This makes remote sensing of these events from both satellites and ground-based observations very difficult, leading to their underrepresentation in these data sets.
2. Frequently observed high levels of fine mode AOD in cloud-dominated skies suggests possible physical mechanisms such as aerosol humidification and cloud processing of aerosols resulting in very high AOD in association with extensive cloud cover in some cases. Meteorological covariation is also possible with convergence (e.g., frontal features, Zhang & Reid, 2009) resulting in higher AOD and also aerosol transport associated with midlatitude cyclonic systems and associated frontal passages. AERONET cloud screening (Version 2) often eliminated many days with the highest AOD that were typically associated with high cloud fraction in this region in winter through summer 2012. High-frequency temporal variation of AOD in the near-cloud environment, plus very few observations per day in cloud gaps, is typically the reason that these observations are eliminated in Version 2 Level 2 AOD data.
3. The new AERONET Version 3 AOD has significantly different cloud screening algorithms than utilized in the Version 2 database. The V3 cloud screening allows more cases of fine mode pollution events that occur on predominately cloudy days to be raised to Level 2 (fully cloud screened and quality assured). Thus, the V3 Level 2 AOD data allows for a more robust and physically realistic characterization of fine mode aerosol events than in V2 Level 2. However, the SDA algorithm applied to Level 1 data (no cloud screening) provides an even more comprehensive assessment of fine mode AOD than Level 2 in both V2 and V3, provided that the L1 data have final calibrations and specific additional quality control checks.
4. Additionally, comparison to AERONET L1 SDA daily average fine mode AOD data shows that MODIS (DT, DB, and MAIAC algorithms) remote sensing of AOD often did not retrieve and/or identify some of the highest fine mode AOD events in this region/season in 2012 (for sites in both Xianghe, China, and Seoul, South Korea). For the Yonsei University site in Seoul all three MODIS algorithms missed the majority of high AOD days likely due in part to the complexity of the terrain with highly urbanized valleys surrounded by densely forested mountains. This is illustrative of difficulties in aerosol remote sensing and the fact that sampling biases in these data sets can be systematic (i.e., will not be canceled out by temporal averaging). Also, NAAPS and MERRA modeling of AOD (assimilating MODIS DT C5 AOD data) compared to L1 SDA fine mode AOD showed that both assimilation models significantly underestimated the magnitude of fine AOD especially for the highest fine mode AOD events that were often associated with significant cloudiness.

5. The relatively frequent satellite retrieval screening out of some high fine mode AOD events in the proximity of clouds in East Asia suggests that the relationships between cloud cover and AOD as determined from satellite data may not be fully characterized in this East Asia region.

More detailed investigation of differences in AERONET Version 2 and 3 AOD data sets, including fine and coarse mode AOD, will be the topic of future studies.

Acknowledgments

We thank Hal Maring (NASA Headquarters) and Steve Platnik (NASA GSFC) for their continuing support and long-term commitment to the AERONET project. MODIS aerosol data are available freely from <https://laadsweb.nascom.nasa.gov>. More information about Deep Blue is available at <https://deepblue.gsfc.nasa.gov>, and more information about Dark Target is at <https://darktarget.gsfc.nasa.gov>. J. S. Reid's and P. Xian contributions were provided by the Office of Naval Research Code 322 (N0001418WX00442). For the Yonsei University team, this research was supported by the National Strategic Project-Fine particle of the National Research Foundation of Korea(NRF) funded by the Ministry of Science and ICT(MSIT), the Ministry of Environment(ME), and the Ministry of Health and Welfare(MOHV). (NRF-2017M3D8A1092022) We also thank two anonymous reviewers and Lorraine Remer for providing valuable reviews that led to strengthening of this paper.

References

- Albrecht, B. A. (1989). Aerosols, cloud microphysics, and fractional cloudiness. *Science*, 245(4923), 1227–1230. <https://doi.org/10.1126/science.245.4923.1227>
- Arola, A., Eck, T. F., Kokkola, H., Pitkanen, M. R. A., & Romakkaniemi, S. (2017). Assessment of cloud-related fine-mode AOD enhancements based on AERONET SDA product. *Atmospheric Chemistry and Physics*, 17(9), 5991–6001. <https://doi.org/10.5194/acp-17-5991-2017>
- Buchard, V., da Silva, A. M., Colarco, P. R., Darmenov, A., Randles, C. A., Govindaraju, R., et al. (2015). Using the OMI aerosol index and absorption aerosol optical depth to evaluate the NASA MERRA aerosol reanalysis. *Atmospheric Chemistry and Physics*, 15(10), 5743–5760. <https://doi.org/10.5194/acp-15-5743-2015>
- Buchard, V., da Silva, A. M., Randles, C. A., Colarco, P., Ferrare, R., Hair, J., et al. (2016). Evaluation of the surface PM 2.5 in version 1 of the NASA MERRA aerosol reanalysis over the United States. *Atmospheric Environment*, 125, 100–111. <https://doi.org/10.1016/j.atmosenv.2015.11.004>
- Buchard, V., Randles, C. A., da Silva, A. M., Darmenov, A., Colarco, P. R., Govindaraju, R., et al. (2017). The MERRA-2 aerosol reanalysis, 1980 onward. Part II: Evaluation and case studies. *Journal of Climate*, 30(17), 6851–6872. <https://doi.org/10.1175/JCLI-D-16-0613.1>
- Chew, B. N., Campbell, J. R., Reid, J. S., Giles, D. M., Welton, E. J., Salinas, S. V., & Liew, S. C. (2011). Tropical cirrus cloud contamination in Sun photometer data. *Atmospheric Environment*, 45(37), 6724–6731. <https://doi.org/10.1016/j.atmosenv.2011.08.017>
- Chin, M., Ginoux, P., Kinne, S., Torres, O., Holben, B. N., Duncan, B. N., et al. (2002). Tropospheric aerosol optical thickness from the GOCART model and comparisons with satellite and Sun photometer measurements. *Journal of the Atmospheric Sciences*, 59(3), 461–483. [https://doi.org/10.1175/1520-0469\(2002\)059%3C0461:TAOTFT%3E2.0.CO;2](https://doi.org/10.1175/1520-0469(2002)059%3C0461:TAOTFT%3E2.0.CO;2)
- Clarke, A. D., Howell, S., Quinn, P. K., Bates, T. S., Ogren, J. A., Andrews, E., et al. (2002). INDOEX aerosol: A comparison and summary of chemical, microphysical, and optical properties observed from land, ship, and aircraft. *Journal of Geophysical Research*, 107(D19), 8033. <https://doi.org/10.1029/2001JD000572>
- Colarco, P., da Silva, A., Chin, M., & Diehl, T. (2010). Online simulations of global aerosol distributions in the NASA GEOS-4 model and comparisons to satellite and ground-based aerosol optical depth. *Journal of Geophysical Research*, 115, D14207. <https://doi.org/10.1029/2009JD012820>
- Dall'Osto, M., Harrison, R. M., Coe, H., & Williams, P. (2009). Real-time secondary aerosol formation during a fog event in London. *Atmospheric Chemistry and Physics*, 9(7), 2459–2469. <https://doi.org/10.5194/acp-9-2459-2009>
- Dubovik, O., & King, M. D. (2000). A flexible inversion algorithm for the retrieval of aerosol optical properties from Sun and sky radiance measurements. *Journal of Geophysical Research*, 105(D16), 20,673–20,696. <https://doi.org/10.1029/2000JD900282>
- Dubovik, O., Sinyuk, A., Lapyonok, T., Holben, B. N., Mishchenko, M., Yang, P., et al. (2006). The application of spheroid models to account for aerosol particle nonsphericity in remote sensing of desert dust. *Journal of Geophysical Research*, 111, D11208. <https://doi.org/10.1029/2005JD006619>
- Dubovik, O., Smirnov, A., Holben, B. N., King, M. D., Kaufman, Y. J., Eck, T. F., & Slutsker, I. (2000). Accuracy assessments of aerosol optical properties retrieved from AERONET Sun and sky-radiance measurements. *Journal of Geophysical Research*, 105(D8), 9791–9806. <https://doi.org/10.1029/2000JD900040>
- Eck, T. F., Holben, B. N., Dubovik, O., Smirnov, A., Goloub, P., Chen, H. B., et al. (2005). Columnar aerosol optical properties at AERONET sites in central eastern Asia and aerosol transport to the tropical mid-Pacific. *Journal of Geophysical Research*, 110, D06202. <https://doi.org/10.1029/2004JD005274>
- Eck, T. F., Holben, B. N., Reid, J. S., Arola, A., Ferrare, R. A., Hostetler, C. A., et al. (2014). Observations of rapid aerosol optical depth enhancements in the vicinity of polluted cumulus clouds. *Atmospheric Chemistry and Physics*, 14, 11,633–11,656. <https://doi.org/10.5194/acp-14-11633-2014>
- Eck, T. F., Holben, B. N., Reid, J. S., Dubovik, O., Smirnov, A., O'Neill, N. T., et al. (1999). Wavelength dependence of the optical depth of biomass burning, urban, and desert dust aerosols. *Journal of Geophysical Research*, 104(D24), 31,333–31,349. <https://doi.org/10.1029/1999JD900923>
- Eck, T. F., Holben, B. N., Reid, J. S., Giles, D. M., Rivas, M. A., Singh, R. P., et al. (2012). Fog- and cloud-induced aerosol modification observed by the Aerosol Robotic Network (AERONET). *Journal of Geophysical Research*, 117, D07206. <https://doi.org/10.1029/2011JD016839>
- Eck, T. F., Holben, B. N., Reid, J. S., O'Neill, N. T., Schafer, J. S., Dubovik, O., et al. (2003). High aerosol optical depth biomass burning events: A comparison of optical properties for different source regions. *Geophysical Research Letters*, 30(20), 2035. <https://doi.org/10.1029/2003GL017861>
- Eck, T. F., Holben, B. N., Reid, J. S., Sinyuk, A., Dubovik, O., Smirnov, A., et al. (2008). Spatial and temporal variability of column-integrated aerosol optical properties in the southern Arabian Gulf and United Arab Emirates in summer. *Journal of Geophysical Research*, 113, D01204. <https://doi.org/10.1029/2007JD008944>
- Eck, T. F., Holben, B. N., Sinyuk, A., Pinker, R. T., Goloub, P., Chen, H., et al. (2010). Climatological aspects of the optical properties of fine/coarse mode aerosol mixtures. *Journal of Geophysical Research*, 115, D19205. <https://doi.org/10.1029/2010JD014002>
- Eck, T. F., Holben, B. N., Ward, D. E., Dubovik, O., Reid, J. S., Smirnov, A., et al. (2001). Characterization of the optical properties of biomass burning aerosols in Zambia during the 1997 ZIBEE field campaign. *Journal of Geophysical Research*, 106(D4), 3425–3448. <https://doi.org/10.1029/2000JD900555>
- Ervens, B., Turpin, B. J., & Weber, R. J. (2011). Secondary organic aerosol formation in cloud droplets and aqueous particles (aqSOA): A review of laboratory, field and model studies. *Atmospheric Chemistry and Physics*, 11, 1069–11,102. <https://doi.org/10.5194/acp-11-1069-2011>
- Ginoux, P., Chin, M., Tegen, I., Prospero, J. M., Holben, B., Dubovik, O., & Lin, S.-J. (2001). Sources and distributions of dust aerosols simulated with the GOCART model. *Journal of Geophysical Research*, 106(D17), 20,255–20,273. <https://doi.org/10.1029/2000JD000053>
- Grandey, B. S., Stier, P., & Wagner, T. M. (2013). Investigating relationships between aerosol optical depth and cloud fraction using satellite, aerosol reanalysis and general circulation model data. *Atmospheric Chemistry and Physics*, 13(6), 3177–3184. <https://doi.org/10.5194/acp-13-3177-2013>

- Gryspeerdt, E., Quaas, J., & Bellouin, N. (2016). Constraining the aerosol influence on cloud fraction. *Journal of Geophysical Research: Atmospheres*, 121, 3566–3583. <https://doi.org/10.1002/2015JD023744>
- Hansen, A. D. A., Benner, W. H., & Novakov, T. (1991). Sulfur-dioxide oxidation in laboratory clouds. *Atmospheric Environment Part A-General Topics*, 25(11), 2521–2530. [https://doi.org/10.1016/0960-1686\(91\)90168-7](https://doi.org/10.1016/0960-1686(91)90168-7)
- Hayden, K. L., Macdonald, A. M., Gong, W., Toom-Sauntry, D., Anlauf, K. G., Leithead, A., et al. (2008). Cloud processing of nitrate. *Journal of Geophysical Research*, 113, D18201. <https://doi.org/10.1029/2007JD009732>
- Hogan, T. F., Liu, M., Ridout, J. S., Peng, M. S., Whitcomb, T. R., Ruston, B. C., et al. (2014). The Navy Global Environmental Model. *Oceanography*, 27(3), 116–125. <https://doi.org/10.5670/oceanog.2014.73>
- Holben, B. N., Eck, T. F., Slutsker, I., Smirnov, A., Sinyuk, A., Schafer, J., et al. (2006). AERONET's version 2.0 quality assurance criteria, remote sensing of atmosphere and clouds. *Proceedings of SPIE The International Society for Optical Engineering*, 6408, 64080Q. <https://doi.org/10.1117/12.706524>
- Holben, B. N., Eck, T. F., Slutsker, I., Tanre, D., Buis, J. P., Setzer, A., et al. (1998). AERONET—A federated instrument network and data archive for aerosol characterization. *Remote Sensing of Environment*, 66(1), 1–16. [https://doi.org/10.1016/S0034-4257\(98\)00031-5](https://doi.org/10.1016/S0034-4257(98)00031-5)
- Holben, B. N., Kim, J., Sano, I., Mukai, S., Eck, T. F., Giles, D. M., et al. (2018). An overview of mesoscale aerosol processes, comparisons, and validation studies from DRAGON networks. *Atmospheric Chemistry and Physics*, 18, 655–671. <https://doi.org/10.5194/acp-18-655-2018>
- Hoppel, W. A., Frick, G. M., Fitzgerald, J. W., & Larson, R. E. (1994). Marine boundary layer measurements of new particle formation and the effects nonprecipitating clouds have on aerosol size distribution. *Journal of Geophysical Research*, 99(D7), 14,443–14,459. <https://doi.org/10.1029/94JD00797>
- Hsu, N. C., Jeong, M. -J., Bettenhausen, C., Sayer, A. M., Hansell, R., Seftor, C. S., et al. (2013). Enhanced Deep Blue aerosol retrieval algorithm: The second generation. *Journal of Geophysical Research: Atmospheres*, 118, 9296–9315. <https://doi.org/10.1002/jgrd.50712>
- Hsu, N. C., Tsay, S. C., King, M. D., & Herman, J. R. (2004). Aerosol properties over bright-reflecting source regions. *IEEE Transactions on Geoscience and Remote Sensing*, 42(3), 557–569. <https://doi.org/10.1109/TGRS.2004.824067>
- Hsu, N. C., Tsay, S. C., King, M. D., & Herman, J. R. (2006). Deep Blue retrievals of Asian aerosol properties during ACE-Asia. *IEEE Transactions on Geoscience and Remote Sensing*, 44(11), 3180–3195. <https://doi.org/10.1109/TGRS.2006.879540>
- Hyer, E. J., Reid, J. S., & Zhang, J. (2011). An over-land aerosol optical depth data set for data assimilation by filtering, correction, and aggregation of MODIS Collection 5 optical depth retrievals. *Atmospheric Measurement Techniques*, 4(3), 379–408. <https://doi.org/10.5194/amt-4-379-2011>
- Intergovernmental Panel on Climate Change (2013). In T. F. Stocker, et al. (Eds.), *Climate change 2013: The physical science basis. Contribution of working group I to the Fifth Assessment Report of the Intergovernmental Panel on Climate Change* (p. 1535). Cambridge, UK and New York: Cambridge University Press. <https://doi.org/10.1017/CBO9781107415324>
- Jeong, M.-J., & Li, Z. (2010). Separating real and apparent effects of cloud, humidity, and dynamics on aerosol optical thickness near cloud edges. *Journal of Geophysical Research*, 115, D00K32. <https://doi.org/10.1029/2009JD013547>
- Johnson, B. T., & Osborne, S. R. (2011). Physical and optical properties of mineral dust aerosol measured by aircraft during the GERBILS campaign. *Quarterly Journal of the Royal Meteorological Society*, 137(658), 1117–1130. <https://doi.org/10.1002/qj.777>
- Joyce, R. J., Janowiak, J. E., Arkin, P. A., & Xie, P. (2004). CMORPH: A method that produces global precipitation estimates from passive microwave and infrared data at high spatial and temporal resolution. *Journal of Hydrometeorology*, 5(3), 487–503. [https://doi.org/10.1175/1525-7541\(2004\)005%3C0487:CAMTPG%3E2.0.CO;2](https://doi.org/10.1175/1525-7541(2004)005%3C0487:CAMTPG%3E2.0.CO;2)
- Kaku, K. C., Reid, J. S., O'Neill, N. T., Quinn, P. K., Coffman, D. J., & Eck, T. F. (2014). Verification and application of the extended spectral deconvolution algorithm (SDA+) methodology to estimate aerosol fine and coarse mode extinction coefficients in the marine boundary layer. *Atmospheric Measurement Techniques*, 7(10), 3399–3412. <https://doi.org/10.5194/amt-7-3399-2014>
- Kaufman, Y. J., Remer, L. A., Tanre, D., Li, R.-R., Kleidman, R., Mattoo, S., et al. (2005). A critical examination of the residual cloud contamination and diurnal sampling effects on MODIS estimates of aerosol over ocean. *IEEE Transactions on Geoscience and Remote Sensing*, 43(12), 2886–2897. <https://doi.org/10.1109/TGRS.2005.858430>
- Kim, S. W., Yoon, S.-C., Kim, J., & Kim, S.-Y. (2007). Seasonal and monthly variations of columnar aerosol optical properties over East Asia determined from multi-year MODIS, LIDAR, and AERONET Sun/sky radiometer measurements. *Atmospheric Environment*, 41(8), 1634–1651. <https://doi.org/10.1016/j.atmosenv.2006.10.044>
- Koo, J.-H. (2008). Optical properties of aerosol in a Megacity, Seoul from ground-based and satellite measurements, (MS thesis). Department of Atmospheric Sciences, The Yonsei University.
- Lee, H. J., & Son, Y.-S. (2016). Spatial variability of AERONET aerosol optical properties and satellite data in South Korea during NASA DRAGON-Asia campaign. *Environmental Science & Technology*, 50(7), 3954–3964. <https://doi.org/10.1021/acs.est.5b04831>
- Levy, R. C., Mattoo, S., Munchak, L. A., Remer, L. A., Sayer, A. M., Patadia, F., & Hsu, N. C. (2013). The Collection 6 MODIS aerosol products over land and ocean. *Atmospheric Measurement Techniques*, 6(11), 2989–3034. <https://doi.org/10.5194/amt-6-2989-2013>
- Levy, R. C., Munchak, L. A., Mattoo, S., Patadia, F., Remer, L. A., & Holz, R. E. (2015). Towards a long-term global aerosol optical depth record: Applying a consistent aerosol retrieval algorithm to MODIS and VIIRS-observed reflectance. *Atmospheric Measurement Techniques*, 8(10), 4083–4110. <https://doi.org/10.5194/amt-8-4083-2015>
- Levy, R. C., Remer, L. A., Mattoo, S., Vermote, E. F., & Kaufman, Y. J. (2007). Second-generation operational algorithm: Retrieval of aerosol properties over land from inversion of Moderate Resolution Imaging Spectroradiometer spectral reflectance. *Journal of Geophysical Research*, 112, D13211. <https://doi.org/10.1029/2006JD007811>
- Li, Z., Eck, T., Zhang, Y., Zhang, Y., Li, D., Li, L., et al. (2014). Observations of residual submicron fine aerosol particles related to cloud and fog processing during a major pollution event in Beijing. *Atmospheric Environment*, 86, 187–192. <https://doi.org/10.1016/j.atmosenv.2013.12.044>
- Lyapustin, A., Korkin, S., Wang, Y., Quayle, B., & Laszlo, I. (2012). Discrimination of biomass burning smoke and clouds in MAIAC algorithm. *Atmospheric Chemistry and Physics*, 12(20), 9679–9686. <https://doi.org/10.5194/acp-12-9679-2012>
- Lyapustin, A., Martonchik, J., Wang, Y., Laszlo, I., & Korkin, S. (2011). Multi-Angle Implementation of Atmospheric Correction (MAIAC): 1. Radiative transfer basis and look-up tables. *Journal of Geophysical Research*, 116, D03210. <https://doi.org/10.1029/2010JD014985>
- Lyapustin, A., Wang, Y., Laszlo, I., Hilker, T., Hall, F., Sellers, P., et al. (2012). Multi-Angle Implementation of Atmospheric Correction for MODIS (MAIAC). 3: Atmospheric correction. *Remote Sensing of Environment*, 127, 385–393. <https://doi.org/10.1016/j.rse.2012.09.002>
- Lyapustin, A., Wang, Y., Laszlo, I., Kahn, R., Korkin, S., Remer, L., et al. (2011). Multi-Angle Implementation of Atmospheric Correction (MAIAC): 2. Aerosol algorithm. *Journal of Geophysical Research*, 116, D03211. <https://doi.org/10.1029/2010JD014986>
- Lyapustin, A., Wang, Y., Xiong, X., Meister, G., Platnick, S., Levy, R., et al. (2014). Scientific impact of MODIS C5 calibration degradation and C6+ improvements. *Atmospheric Measurement Techniques*, 7(12), 4353–4365. <https://doi.org/10.5194/amt-7-4353-2014>

- Lynch, P., Reid, J. S., Westphal, D. L., Zhang, J., Hogan, T. F., Hyer, E. J., et al. (2016). An 11-year global gridded aerosol optical thickness reanalysis (v1.0) for atmospheric and climate sciences. *Geoscientific Model Development*, 9(4), 1489–1522. <https://doi.org/10.5194/gmd-9-1489-2016>
- Marshak, A., Wen, G., Coakley, J. A. Jr., Remer, L. A., Loeb, N. G., & Cahalan, R. F. (2008). A simple model for the cloud adjacency effect and the apparent bluing of aerosols near clouds. *Journal of Geophysical Research*, 113, D14S17. <https://doi.org/10.1029/2007JD009196>
- Martins, V. S., Lyapustin, A., de Carvalho, L. A. S., Barbosa, C. C. F., & Novo, E. M. L. M. (2017). Validation of high-resolution MAIAC aerosol product over South America. *Journal of Geophysical Research: Atmospheres*, 122, 7537–7559. <https://doi.org/10.1002/2016JD026301>
- Munger, J. W., Tiller, C., & Hoffmann, M. R. (1986). Identification of hydroxymethanesulfonate in fog water. *Science*, 231(4735), 247–249. <https://doi.org/10.1126/science.231.4735.247>
- Noone, K. J., Ogren, J. A., Hallberg, A., Heintzenberg, J., Ström, J., Hansson, H.-C., et al. (1992). Changes in aerosol size- and phase distributions due to physical and chemical processes in fog. *Tellus Series B: Chemical and Physical Meteorology*, 44(5), 489–504. <https://doi.org/10.1034/j.1600-0889.1992.t01-4-00004.x>
- O'Neill, N. T., Eck, T. F., Holben, B. N., Smirnov, A., Dubovik, O., & Royer, A. (2001). Bimodal size distribution influences on the variation of Ångström derivatives in spectral and optical depth space. *Journal of Geophysical Research*, 106(D9), 9787–9806. <https://doi.org/10.1029/2000JD900245>
- O'Neill, N. T., Eck, T. F., Reid, J. S., Smirnov, A., & Pancrati, O. (2008). Coarse mode optical information retrievable using ultraviolet to short-wave infrared Sun photometry: Application to United Arab Emirates Unified Aerosol Experiment data. *Journal of Geophysical Research*, 113, D05212. <https://doi.org/10.1029/2007JD009052>
- O'Neill, N. T., Eck, T. F., Smirnov, A., Holben, B. N., & Thulasiraman, S. (2003). Spectral discrimination of coarse and fine mode optical depth. *Journal of Geophysical Research*, 108(D17), 4559. <https://doi.org/10.1029/2002JD00297>
- O'Neill, N. T., Thulasiraman, S., Eck, T. F., & Reid, J. S. (2005). Robust optical features of fine mode size distributions: Application to the Quebec smoke event of 2002. *Journal of Geophysical Research*, 110, D11207. <https://doi.org/10.1029/2004JD005157>
- Pope, C. A. III (2000). Epidemiology of fine particulate air pollution and human health: Biologic mechanisms and who's at risk? *Environmental Health Perspectives*, 108, 713–723.
- Pueschel, R. F., Russell, P. B., Allen, D. A., Ferry, G. V., Snetsinger, K. G., Livingston, J. M., & Verma, S. (1994). Physical and optical properties of the Pinatubo volcanic aerosol: Aircraft observations with impactors and a Sun-tracking photometer. *Journal of Geophysical Research*, 99(D6), 12,915–12,922. <https://doi.org/10.1029/94JD00621>
- Qu, W., Wang, J., Zhang, X., Sheng, L., & Wang, W. (2016). Opposite seasonality of the aerosol optical depth and the surface particulate matter concentration over the North China Plain. *Atmospheric Environment*, 127, 90–99. <https://doi.org/10.1016/j.atmosenv.2015.11.061>
- Quaas, J., Stevens, B., Stier, P., & Lohmann, U. (2010). Interpreting the cloud cover—Aerosol optical depth relationship found in satellite data using a general circulation model. *Atmospheric Chemistry and Physics*, 10(13), 6129–6135. <https://doi.org/10.5194/acp-10-6129-2010>
- Randles, C. A., da Silva, A. M., Buchard, V., Colarco, P. R., Darmenov, A., Govindaraju, R., et al. (2017). The MERRA-2 aerosol reanalysis, 1980 onward. Part I: System description and data assimilation evaluation. *Journal of Climate*, 30(17), 6823–6850. <https://doi.org/10.1175/JCLI-D-16-0609.1>
- Reid, J. S., Brooks, B., Crahan, K. K., Hegg, D. A., Eck, T. F., O'Neill, N., et al. (2006). Reconciliation of coarse mode sea-salt aerosol particle size measurements and parameterizations at a subtropical ocean receptor site. *Journal of Geophysical Research*, 111, D02202. <https://doi.org/10.1029/2005JD006200>
- Reid, J. S., Eck, T. F., Christopher, S. A., Hobbs, P. V., & Holben, B. N. (1999). Use of the Ångström exponent to estimate the variability of optical and physical properties of aging smoke particles in Brazil. *Journal of Geophysical Research*, 104, 27,473–27,489. <https://doi.org/10.1029/1999JD900833>
- Reid, J. S., Hyer, E. J., Johnson, R. S., Holben, B. N., Yokelson, R. J., Zhang, J., et al. (2013). Observing and understanding the Southeast Asian aerosol system by remote sensing: An initial review and analysis for the Seven Southeast Asian Studies (7SEAS) program. *Atmospheric Research*, 122, 403–468. <https://doi.org/10.1016/j.atmosres.2012.06.005>
- Reid, J. S., Hyer, E. J., Prins, E. M., Westphal, D. L., Zhang, J., Wang, J., et al. (2009). Global monitoring and forecasting of biomass-burning smoke: Description of and lessons from the Fire Locating and Modeling of Burning Emissions (FLAMBE) program. *IEEE Journal of Selected Topics in Applied Earth Observations and Remote Sensing*, 2(3), 144–162. <https://doi.org/10.1109/JSTARS.2009.2027443>
- Reid, J. S., Koppmann, R., Eck, T., & Eleuterio, D. (2005). A review of biomass burning emissions Part II: Intensive physical properties of biomass burning particles. *Atmospheric Chemistry and Physics*, 5, 799–825.
- Reid, J. S., Reid, E. A., Walker, A., Piketh, S., Cliff, S., Al Mandoos, A., et al. (2008). Dynamics of southwest Asian dust particle size characteristics with implications for global dust research. *Journal of Geophysical Research*, 113, D14212. <https://doi.org/10.1029/2007JD009752>
- Remer, L. A., Mattoo, S., Levy, R. C., & Munchak, L. A. (2013). MODIS 3 km aerosol product: Algorithm and global perspective. *Atmospheric Measurement Techniques*, 6(7), 1829–1844. <https://doi.org/10.5194/amt-6-1829-2013>
- Rienecker, M. M., Suarez, M. J., Gelaro, R., Todling, R., Bacmeister, J., Liu, E., et al. (2011). MERRA: NASA's Modern-Era Retrospective Analysis for Research and Applications. *Journal of Climate*, 24(14), 3624–3648.
- Rubin, J. I., Reid, J. S., Hansen, J. A., Anderson, J. L., Holben, B. N., Xian, P., et al. (2017). Assimilation of AERONET and MODIS AOT observations using variational and ensemble data assimilation methods and its impact on aerosol forecasting skill. *Journal of Geophysical Research: Atmospheres*, 122, 4967–4992. <https://doi.org/10.1002/2016JD026067>
- Saide, P. E., Carmichael, G. R., Liu, Z., Schwartz, C. S., Lin, H. C., da Silva, A. M., & Hyer, E. (2013). Aerosol optical depth assimilation for a size-resolved sectional model: Impacts of observationally constrained, multi-wavelength and fine mode retrievals on regional scale analyses and forecasts. *Atmospheric Chemistry and Physics*, 13(20), 10,425–10,444.
- Sano, I., Mukai, S., Nakata, M., & Holben, B. N. (2016). Regional and local variations in atmospheric aerosols using ground-based Sun photometry during Distributed Regional Aerosol Gridded Observation Networks (DRAGON) in 2012. *Atmospheric Chemistry and Physics*, 16, 14,795–14,803. <https://doi.org/10.5194/acp-16-14795-2016>
- Sayer, A. M., Hsu, N. C., & Bettenhausen, C. (2015). Implications of MODIS bow-tie distortion on aerosol optical depth retrievals, and techniques for mitigation. *Atmospheric Measurement Techniques*, 8(12), 5277–5288. <https://doi.org/10.5194/amt-8-5277-2015>
- Sayer, A. M., Hsu, N. C., Bettenhausen, C., & Jeong, M.-J. (2013). Validation and uncertainty estimates for MODIS Collection 6 “Deep Blue” aerosol data. *Journal of Geophysical Research: Atmospheres*, 118, 7864–7872. <https://doi.org/10.1002/jgrd.50600>
- Sayer, A. M., Hsu, N. C., Bettenhausen, C., Jeong, M.-J., & Meister, G. (2015). Effect of MODIS Terra radiometric calibration improvements on Collection 6 Deep Blue aerosol products: Validation and Terra/Aqua consistency. *Journal of Geophysical Research: Atmospheres*, 120, 12,157–12,174. <https://doi.org/10.1002/2015JD023878>
- Sayer, A. M., Munchak, L. A., Hsu, N. C., Levy, R. C., Bettenhausen, C., & Jeong, M.-J. (2014). MODIS Collection 6 aerosol products: Comparison between Aqua's e-Deep Blue, Dark Target, and “merged” data sets, and usage recommendations. *Journal of Geophysical Research: Atmospheres*, 119, 13,965–13,989. <https://doi.org/10.1002/2014JD022453>

- Sessions, W. R., Reid, J. S., Benedetti, A., Colarco, P. R., da Silva, A., Lu, S., et al. (2015). Development towards a global operational aerosol consensus: basic climatological characteristics of the International Cooperative for Aerosol Prediction Multi-Model Ensemble (ICAP-MME). *Atmospheric Chemistry and Physics*, 15, 335–362. <https://doi.org/10.5194/acp-15-335-2015>
- Schmid, B., Michalsky, J., Halthore, R., Beauharnois, M., Harrison, L., Livingston, J., et al. (1999). Comparison of aerosol optical depth from four solar radiometers during the fall 1997 ARM intensive observation period. *Geophysical Research Letters*, 26(17), 2725–2728. <https://doi.org/10.1029/1999GL900513>
- Schutgens, N. A. J., Partridge, D. G., & Stier, P. (2016). The importance of temporal collocation for the evaluation of aerosol models with observations. *Atmospheric Chemistry and Physics*, 16(2), 1065–1079. <https://doi.org/10.5194/acp-16-1065-2016>
- Shi, Y. (2015). Critical evaluations of MODIS and MISR satellite aerosol products for aerosol modeling applications, (PhD dissertation). University of North Dakota.
- Shi, Y., Zhang, J., Reid, J. S., Liu, B., & Hyer, E. J. (2014). Critical evaluation of cloud contamination in the MISR aerosol products using MODIS cloud mask products. *Atmospheric Measurement Techniques*, 7(6), 1791–1801. <https://doi.org/10.5194/amt-7-1791-2014>
- Sinyuk, A., Holben, B. N., Smirnov, A., Eck, T. F., Slutsker, I., Schafer, J. S., et al. (2012). Assessment of error in aerosol optical depth measured by AERONET due to aerosol forward scattering. *Geophysical Research Letters*, 39, L23806. <https://doi.org/10.1029/2012GL053894>
- Smirnov, A., Holben, B. N., Dubovik, O., Frouin, R., Eck, T. F., & Slutsker, I. (2003). Maritime component in aerosol optical models derived from Aerosol Robotic Network data. *Journal of Geophysical Research*, 108(D1), 4033. <https://doi.org/10.1029/2002JD002701>
- Smirnov, A., Holben, B. N., Eck, T. F., Dubovik, O., & Slutsker, I. (2000). Cloud screening and quality control algorithms for the AERONET data base. *Remote Sensing of Environment*, 73(3), 337–349. [https://doi.org/10.1016/S0034-4257\(00\)00109-7](https://doi.org/10.1016/S0034-4257(00)00109-7)
- Smirnov, A., Zhuravleva, T. B., Segal-Rosenheimer, M., & Holben, B. N. (2018). Limitations of AERONET SDA product in presence of cirrus clouds. *Journal of Quantitative Spectroscopy and Radiative Transfer*, 206, 338–341. <https://doi.org/10.1016/j.jqsrt.2017.12.007>
- Su, W., Schuster, G. L., Loeb, N. G., Rogers, R. R., Ferrare, R. A., Hostetler, C. A., et al. (2008). Aerosol and cloud interaction observed from high spectral resolution lidar data. *Journal of Geophysical Research*, 113, D24202. <https://doi.org/10.1029/2008JD010588>
- Superczynski, S., Kondragunta, S., & Lyapustin, A. (2017). Evaluation of the Multi-Angle Implementation of Atmospheric Correction (MAIAC) aerosol algorithm through intercomparison with VIIRS aerosol products and AERONET. *Journal of Geophysical Research: Atmospheres*, 122, 3005–3022. <https://doi.org/10.1002/2016JD025720>
- Tackett, J. L., & Di Girolamo, L. (2009). Enhanced aerosol backscatter adjacent to tropical trade wind clouds revealed by satellite-based lidar. *Geophysical Research Letters*, 36, L14804. <https://doi.org/10.1029/2009GL039264>
- Toller, G., Xiaoxiong, X., Sun, J., Wenny, B. N., Geng, X., Kuyper, J., et al. (2013). Terra and Aqua Moderate-Resolution Imaging Spectroradiometer Collection 6 level 1b algorithm. *Journal of Applied Remote Sensing*, 7(1), 073557. <https://doi.org/10.1117/1.JRS.7.073557>
- Várnai, T., & Marshak, A. (2009). MODIS observations of enhanced clear sky reflectance near clouds. *Geophysical Research Letters*, 36, L06807. <https://doi.org/10.1029/2008GL037089>
- Várnai, T., & Marshak, A. (2011). Global CALIPSO observations of aerosol changes near clouds. *IEEE Geoscience and Remote Sensing Letters*, 8(1), 19–23. <https://doi.org/10.1109/LGRS.2010.2049982>
- Westphal, D. L., Toon, O. B., & Carlson, T. N. (1987). A two-dimensional numerical investigation of the dynamics and microphysics of Saharan dust storms. *Journal of Geophysical Research*, 92(D3), 3027–3049. <https://doi.org/10.1029/JD092iD03p03027>
- Whiteaker, J. R., & Prather, K. A. (2003). Hydroxymethanesulfonate as a tracer for fog processing of individual aerosol particles. *Atmospheric Environment*, 37(8), 1033–1043. [https://doi.org/10.1016/S1352-2310\(02\)01029-4](https://doi.org/10.1016/S1352-2310(02)01029-4)
- Witek, M. L., Flatau, P. J., Quinn, P. K., & Westphal, D. L. (2007). Global sea-salt modeling: Results and validation against multicampaign shipboard measurements. *Journal of Geophysical Research*, 112, D08215. <https://doi.org/10.1029/2006JD007779>
- Xian, P., Reid, J. S., Turk, J. F., Hyer, E. J., & Westphal, D. L. (2009). Impact of models versus satellite measured tropical precipitation on regional smoke optical thickness in an aerosol transport model. *Geophysical Research Letters*, 36, L16805. <https://doi.org/10.1029/2009GL038823>
- Yang, M., Howell, S. G., Zhuang, J., & Huebert, B. J. (2009). Attribution of aerosol light absorption to black carbon, brown carbon, and dust in China—Interpretations of atmospheric measurements during EASTAIRE. *Atmospheric Chemistry and Physics*, 9(6), 2035–2050. <https://doi.org/10.5194/acp-9-2035-2009>
- Yang, W., Marshak, A., Várnai, T., & Liu, Z. (2012). Effect of CALIPSO cloud-aerosol discrimination (CAD) confidence levels on observations of aerosol properties near clouds. *Atmospheric Research*, 116, 134–141. <https://doi.org/10.1016/j.atmosres.2012.03.013>
- Yi, B., Rapp, A. D., Yang, P., Baum, B. A., & King, M. D. (2017). A comparison of aqua MODIS ice and liquid water cloud physical and optical properties between Collection 6 and collection 5.1: Pixel-to-pixel comparisons. *Journal of Geophysical Research: Atmospheres*, 122, 4528–4549. <https://doi.org/10.1002/2016JD025586>
- Zhang, J., & Reid, J. S. (2006). MODIS aerosol product analysis for data assimilation: Assessment of Level 2 aerosol optical thickness retrievals. *Journal of Geophysical Research*, 111, D22207. <https://doi.org/10.1029/2005JD006898>
- Zhang, J., & Reid, J. S. (2009). An analysis of clear sky and contextual biases using an operational over ocean MODIS aerosol product. *Geophysical Research Letters*, 36, L15824. <https://doi.org/10.1029/2009GL038723>
- Zhang, J., Reid, J. S., & Holben, B. N. (2005). An analysis of potential cloud artifacts in MODIS over ocean aerosol optical thickness products. *Geophysical Research Letters*, 32, L15803. <https://doi.org/10.1029/2005GL023254>
- Zhang, J., Reid, J. S., Westphal, D. L., Baker, N. L., & Hyer, E. J. (2008). A system for operational aerosol optical depth data assimilation over global oceans. *Journal of Geophysical Research*, 113, D10208. <https://doi.org/10.1029/2007JD009065>